Title

Single-cell genomics reveals region-specific developmental trajectories underlying neuronal diversity in the human hypothalamus.

Journal

Science Advances, 9(45)

Authors

Herb, Brian
Glover, Hannah
Bhaduri, Aparna
et al.

Publication Date

2023-11-10

DOI

10.1126/sciadv.adf6251

Peer reviewed

NEUROSCIENCE

Single-cell genomics reveals region-specific developmental trajectories underlying neuronal diversity in the human hypothalamus

Brian R. Herb[1,2,3,4]†, Hannah J. Glover[5]†, Aparna Bhaduri[6], Carlo Colantuoni[1,7], Tracy L. Bale[8], Kimberly Siletti[9], Rebecca Hodge[10], Ed Lein[10], Arnold R. Kriegstein[11,12], Claudia A. Doege[13]*, Seth A. Ament[1,3,4,14]*

The development and diversity of neuronal subtypes in the human hypothalamus has been insufficiently characterized. To address this, we integrated transcriptomic data from 241,096 cells (126,840 newly generated) in the prenatal and adult human hypothalamus to reveal a temporal trajectory from proliferative stem cell populations to mature hypothalamic cell types. Iterative clustering of the adult neurons identified 108 robust transcriptionally distinct neuronal subtypes representing 10 hypothalamic nuclei. Pseudotime trajectories provided insights into the genes driving formation of these nuclei. Comparisons to single-cell transcriptomic data from the mouse hypothalamus suggested extensive conservation of neuronal subtypes despite certain differences in species-enriched gene expression. The uniqueness of hypothalamic neuronal lineages was examined developmentally by comparing excitatory lineages present in cortex and inhibitory lineages in ganglionic eminence, revealing both distinct and shared drivers of neuronal maturation across the human forebrain. These results provide a comprehensive transcriptomic view of human hypothalamus development through gestation and adulthood at cellular resolution.

INTRODUCTION

The hypothalamus is a small but anatomically complex brain region that controls a large variety of evolutionally requisite physiological and homeostatic functions, including body temperature, circadian rhythms, sleep, stress responses, satiety, and hunger, as well as aspects of mood, social behavior, and memory (*1*–*3*). These functions are subdivided among specialized neuronal subtypes, which are organized into distinct anatomical nuclei (*4*–*33*). Environmental and genetic perturbations to hypothalamic development result in long-lasting changes in physiology and behavior (*34*–*42*) and are thought to contribute to risk for human diseases including obesity, anxiety, and depression (*43*–*45*). These clinical consequences motivate deeper investigation into the timing and regulation of hypothalamic development leading to the neuronal subtypes of the adult hypothalamus. However, much of what we know about hypothalamic development comes from animal models (*2*–*11*, *34*, *46*–*48*). While the developmental timing and regional diversity of human hypothalamic neurons have been extensively characterized using classical markers (*49*–*51*), more precise atlases for their molecular identities enabled by single-cell genomics have only recently begun to be characterized and were restricted to time points in early- to mid-gestation (*52*, *53*). Here, we present single-cell transcriptomics of the prenatal [gestational weeks (GW) 6 to 25] and adult human hypothalamus to define its transcriptional cell types and developmental trajectories into adulthood.

RESULTS

An atlas of neuronal and non-neuronal lineages in the developing human hypothalamus

We performed 10X Genomics single-cell RNA sequencing (scRNA-seq) of the prenatal hypothalamus from 11 human fetuses (4 female, 7 male) at ~6 to 25 GW (GW6 to GW7, GW10, GW16, GW18 to GW20, GW22, and GW25), yielding 40,927 high-quality single-cell transcriptomes (Fig. 1A and table S1). In addition, we performed single-nucleus RNA sequencing (snRNA-seq) of neurons from the post-mortem hypothalamus of three neurotypical donors (males, 29, 42, and 50 years of age; Fig. 1A and fig. S1), yielding 85,913 high-quality single-nucleus transcriptomes. Both the prenatal and adult samples were collected in parallel with samples from additional brain regions in the same donors, some of which have been reported previously or in parallel with this study (*54*–*57*).

We integrated the 40,927 prenatal hypothalamic cells with 114,256 cells from Zhou *et al.* (*52*) (containing GW7 to GW8,

[1]Institute for Genome Sciences, University of Maryland School of Medicine, Baltimore, MD, USA. [2]Department of Pharmacology, University of Maryland School of Medicine, Baltimore, MD, USA. [3]UM-MIND, University of Maryland School of Medicine, Baltimore, MD, USA. [4]Kahlert Institute for Addiction Medicine, University of Maryland School of Medicine, Baltimore, MD, USA. [5]Naomi Berrie Diabetes Center, Columbia Stem Cell Initiative, Department of Pediatrics, Columbia University Irving Medical Center, New York, NY, USA. [6]Department of Biological Chemistry, University of California, Los Angeles, Los Angeles, CA, USA. [7]Department of Neurology, Johns Hopkins University School of Medicine, Baltimore, MD, USA. [8]Department of Psychiatry, University of Colorado School of Medicine, Aurora, CO, USA. [9]Department of Medical Biochemistry and Biophysics, Karolinska Institutet, Stockholm, Sweden. [10]Allen Institute for Brain Science, Seattle, WA 98109. [11]Department of Neurology, University of California, San Francisco, San Francisco, CA, USA. [12]The Eli and Edythe Broad Center of Regeneration Medicine and Stem Cell Research, University of California, San Francisco, CA, USA. [13]Naomi Berrie Diabetes Center, Columbia Stem Cell Initiative, Department of Pathology and Cell Biology, Columbia University Irving Medical Center, New York, NY, USA. [14]Maryland Psychiatric Research Center, Department of Psychiatry, University of Maryland School of Medicine, Baltimore, MD, USA.
*Corresponding author. Email: sament@som.umaryland.edu (S.A.A.); cad2114@cumc.columbia.edu (C.A.D.)
†These authors contributed equally to this work.

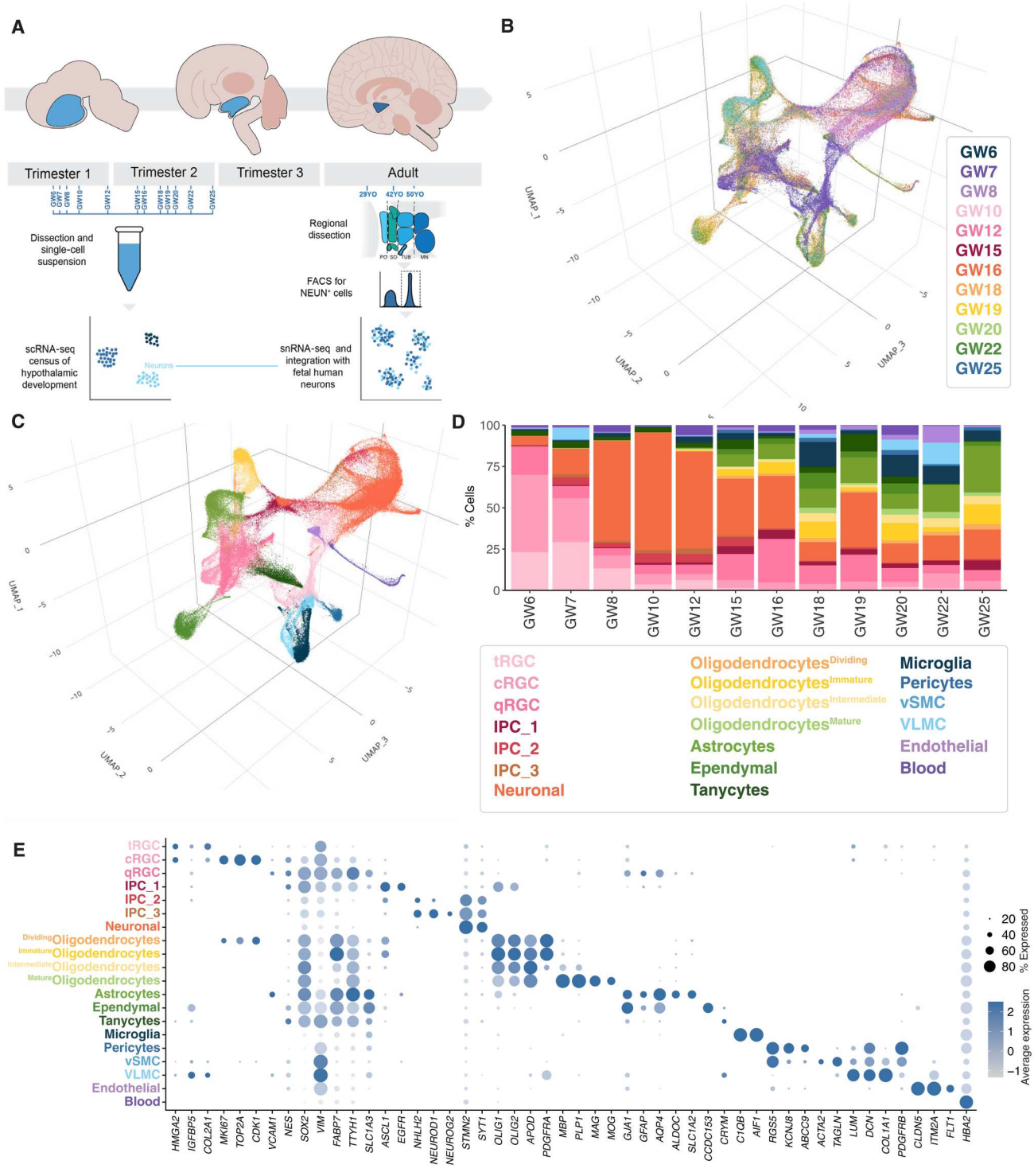

Fig. 1. Neuronal and non-neuronal lineages across the developing human hypothalamus. (**A**) Overview of sample collection, including single-cell RNA-seq analysis of the first and second trimester prenatal hypothalamus plus snRNA-seq from adult hypothalamic neurons dissected into four regions. FACS, fluorescence-activated cell sorting. (**B**) Three-dimensional (3D) UMAP (https://tinyurl.com/3fxxy3yj) showing integrated samples of the prenatal hypothalamic samples including trimester 1 (GW6, GW7, GW8, GW10, and GW12) and trimester 2 (GW15, GW16, GW18, GW19, GW20, GW22, and GW25). (**C**) 3D UMAP (https://tinyurl.com/3vnc9fym) showing samples after clustering to show cell subpopulations including transitionary radial glia cell (tRGC), cycling radial glia cell (cRGC), and quiescent radial glia cell (qRGC), as well as three populations of intermediate progenitor cells (IPCs). (**D**) Stacked plot showing distribution of cell subpopulation across samples. (**E**) Dot plot showing expression of key marker genes.

GW10, GW12, GW15, GW18, and GW20; Fig. 1B and fig. S2) to generate a comprehensive atlas spanning from the first trimester to the end of the second trimester. Cell populations were annotated (tables S2 and S3) on the basis of established marker genes from prior studies (*4*, *47*, *54*, *57*–*59*). We identified 20 broad cell classes, including radial glia, intermediate progenitors, neurons, astrocytes, microglia, and oligodendrocytes, as well as hypothalamus-specific populations such as ependymocytes and tanycytes (Fig. 1, C to E; fig. S2B; and tables S3 and S4).

Cell-type distributions shifted over developmental time (Fig. 1D and fig. S2, B and C). The earliest time points, GW6 and GW7, were composed largely of three radial glia populations: transitional state radial glia cells (tRGCs; *VIM/HMGA2/COL2A1*$^+$), quiescent radial glia cells (qRGCs; *SOX2/VIM/HES1/FABP7/SLC1A3/TTYH1*$^+$), and cycling radial glia cells (cRGCs; *SOX2/VIM/HES1/MKI67/HMGA2/TOP2A/CDK1*$^+$), similar to those reported previously (*47*, *53*). Three additional progenitor populations—intermediate progenitors cells—were present starting from GW7, including an *ASCL1/EGFR/OLIG1/OLIG2*$^+$ population that did not express mature neuronal markers (*STMN2/SYT1*$^-$) and two additional *STMN2/SYT1*$^+$ intermediate progenitor clusters: an *ASCL1/NEUROG2/NEUROD1*$^+$ population and a *NEUROG2/NEUROD1/NHLH2*$^+$ population. From GW6, we also noted a population of *RAX/CRYM*$^+$ tanycytes, a specialized radial glia-like cell type lining the third ventricle. *CCDC153/FOXJ1*$^+$ ependymocytes, which are functionally and spatially related to tanycytes, emerge from GW15.

A small population of post-mitotic neurons (*STMN2/SYT1*$^+$) were present from the earliest stages, becoming more prevalent at the GW8 to GW12 time points. There were some disparities in the proportion of neurons in matched time points from our study and the work by Zhou *et al.* (*52*) (fig. S2C), suggesting differences in staging of the fetuses between the two studies. The data published by Zhou *et al.* (*52*) show that 17.0% of the sample was composed of post-mitotic neurons compared to only 6.4% of our GW7 sample (fig. S2, B and C). This disparity was also evident in matched samples at GW10 (Zhou: 79.7%; Herb: 56.3%), and was reversed at GW18 (Zhou: 5.3%; Herb: 53.5%) and GW20 (Zhou: 6.7%; Herb: 42.2%), primarily due to the predominance of emerging glial populations in the Zhou *et al.* (*52*) data. Despite these differences in proportion, all of the populations were reproducible across datasets.

A wave of gliogenesis occurred following the wave of neurogenesis, spanning from GW15 to GW25 (Fig. 1, D and E). Both the astrocyte (*GJA1/GFAP/AQP4*$^+$) and most of the oligodendrocyte lineage (*OLIG1/OLIG2/APOD*$^+$) present by GW15. Mature oligodendrocytes were present by GW18 (*MAG/MOG*$^+$). Microglia (*C1QB/AIF1*$^+$) were present from GW12 but were most abundant from GW18.

Supporting cells such as pericytes (*KCNJ8/ABCC9*$^+$), vascular smooth muscle cells (vSMC; *ACTA2/TAGLN*$^+$), vascular leptomeningeal cells (VLMC; *LUM/DCN*$^+$), endothelial cells (*CLDN5/ITM2A*$^+$), and erythrocytes (*HBA2*$^+$) represented a small proportion of the cells throughout GW6 to GW25 (Fig. 1, D and E).

Neuronal diversity in the adult hypothalamus

We integrated *STMN2/SYT1*$^+$ neurons and intermediate progenitors from GW10 to adulthood to characterize both neuronal diversity and neurogenic trajectories, including n = 35,908 prenatal cells and n = 85,913 adult hypothalamic cells (Fig. 2, A and B, and table S5). Time points earlier than GW10 and earlier-stage progenitor populations were excluded from this analysis due to difficulty in placing them into a unified, detailed trajectory. The resulting integration positioned the prenatal populations toward the center of the Uniform Manifold Approximation and Projection (UMAP) plot with the adult samples radiating from this center (Fig. 2B), reflecting maturation from prenatal to adult populations. The glutaminergic (*SLC17A6*$^+$), GABAergic (*SLC32A1*$^+$), and histaminergic (*HDC*$^+$) cell populations were delineated across the UMAP (Fig. 2C).

We applied an iterative hierarchical clustering approach to obtain a more detailed atlas of neuronal subtypes, focusing on the mature neurons from the adult hypothalamus (Fig. 2D; fig. S3, A to C; and table S6). Clustering was performed at increasing resolutions and then aggregated using a multiresolution reconciled tree to produce nested cluster annotations at 15 levels of resolution, resulting in 6 transcriptionally distinct human neuronal clusters (henceforth, "H6") at the highest level and 369 clusters (H369) at the deepest level (fig. S3). A stopping distance was set to ensure that clusters were composed of cells from multiple donors (table S7) and had at least 10 differentially expressed genes. To further assess the cluster stability, we calculated a subsampling, bootstrapped silhouette score to determine cluster stability. This indicated maximal cluster stability at 108 clusters (H108; Fig. 2D and fig. S3).

Clusters were annotated at multiple levels (H6, H53, H108, and H369) based on their marker genes (fig. S3 and table S6), taking into consideration the subregions dissected for each sample. These annotations classified neurons according to the neurotransmitters they produce, including GABAergic (*SLC32A1*$^+$), glutaminergic (*SLC17A6*$^+$), and histaminergic (*HDC*$^+$) subtypes. Clusters were also annotated to their predicted subregion of origin, including 10 hypothalamic nuclei (Fig. 2, D and E; figs. S3 to S5; and tables S8 to S10): the Arcuate (ARC; representative marker: *TBX3*$^+$), tuberomammillary terminal (TM; representative markers: *TBX3/HDC*$^+$), paraventricular nucleus of the hypothalamus (PVH; representative markers: *SIM1/POU3F2*$^+$), ventromedial nucleus of the hypothalamus (VMH; representative markers: *NR5A1/FEZF1*$^+$), dorsomedial nucleus of the hypothalamus (DMH; representative markers: *PPP1R17/GPR50*$^+$), lateral hypothalamus (LH; representative markers: *HCRT/PDYN/LHX9*$^+$), suprachiasmatic nucleus (SCN; representative markers: *RGS16/RELN*$^+$), supramammillary nucleus (SMN; representative marker: *LMX1A*$^+$), mammillary nucleus (MN; representative marker: *FOXB1*$^+$), and preoptic area (PO; representative markers: *ARX/NFIX*$^+$). Notably, cells of the zona incerta (ZI; representative marker: *MEIS2*$^+$), a region of the subthalamus, were also identified. Nuclei annotations were based on established markers from the literature [tables S6 and S8 and localized gene expression in the Allen Brain Atlas (fig. S4)]. Not all human nuclei can be reliably identified due to a lack of distinguishing marker genes and/or species specific differences. Our annotations could not readily discern the supraoptic hypothalamus, anterior hypothalamus, or posterior hypothalamus, and these nuclei are expected to be encompassed within the PVH, SCN, or SMN annotations, respectively.

Consistently across the H53 (fig. S3B), H108 (Fig. 2, D to E; fig. S3E; and tables S12 and S13), and H369 (fig. S3C and table S14) levels of resolution, >80% of cells and >90% of clusters were

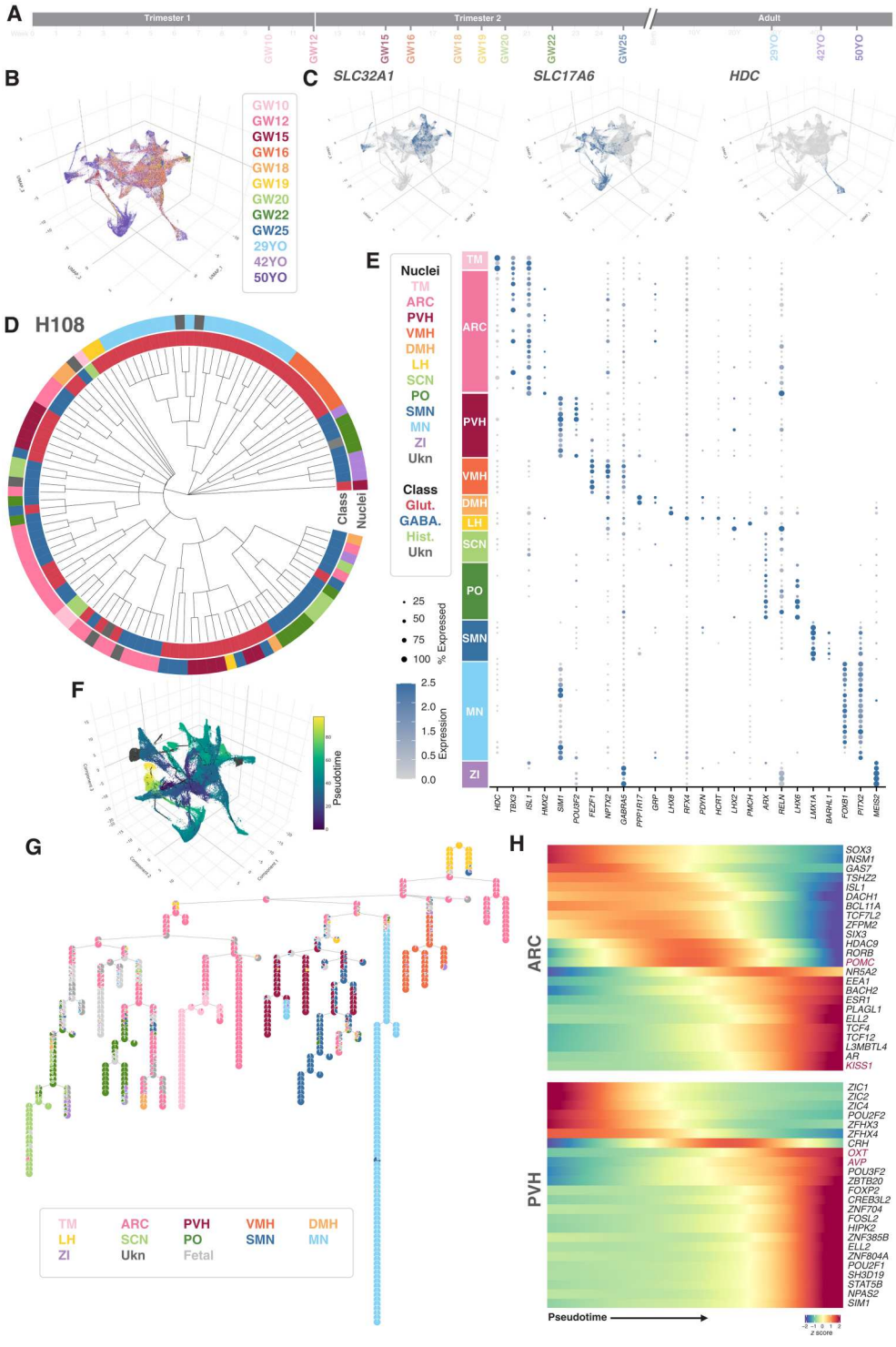

Fig. 2. Neuronal trajectories across development and the adult human hypothalamus. (**A**) sc/snRNAseq of postmitotic neurons from prenatal (GW10 to GW25) and adult hypothalamus. (**B**) 3D UMAP (https://tinyurl.com/2sft9bk3) for prenatal and adult hypothalamic neurons, showing overlay of samples by time point. (**C**) Dispersed expression of GABAergic (*SLC32A1*), glutaminergic (*SLC17A6*), and histaminergic (*HDC*) cell populations. (**D**) Fifteen levels of iterative clustering were used to find the maximum number of clusters (H369 clusters) that retained unique gene expression and were distributed across at least two donors. After assessing cluster stability (fig. S3D), these were annotated at the H108 level by expression (fig. S5) of marker genes in fig. S3 and table S8. Nuclei included the tuberomammillary terminal (TM), arcuate (ARC), paraventricular nucleus of the hypothalamus (PVH), ventromedial nucleus of the hypothalamus (VMH), dorsomedial nucleus of the hypothalamus (DMH), lateral hypothalamus (LH), suprachiasmatic nucleus (SCN), supramammillary nucleus (SMN), mammillary nucleus (MN), preoptic area (PO), and the zona incerta (ZI). These were organized by hierarchical clustering and visualized as a dendrogram overlaid with the neuronal classes (inner) and the 11 anatomical regions (outer). (**E**) Dot plot showing expression of key marker genes for each nuclei. (**F**) Monocle3 pseudotime (https://tinyurl.com/5ebjuhcz) trajectories rooted at the vertex with the highest proportion of cells from the earliest time point (GW10). (**G**) A lineage tree was derived from the Monocle3 pseudotime trajectory. Adult nuclei assignments from the H108 level were overlaid on the trajectory, and prenatal assignments were extrapolated where they contributed to a vertex with a robust percentage of adult neuronal assignments. (**H**) Heatmap of TF and NP expression (normalized *z* score) across pseudotime for the ARC branch, showing genes upstream of POMC and KISS1 (top), and the PVH branch for genes upstream of OXT and AVP (bottom).

assigned to specific nuclei. We attempted to validate these subregion assignments using in situ hybridization data from the Allen Brain Atlas and scCoco (*60*), confirming 66% of clusters at the H53 level despite differences in species and technology (fig. S6 and table S11). At the most granular level (H369), all PVH, VMH, LH, and MN clusters were assigned as glutamatergic neurons, all SCN and ZI clusters were assigned as GABAergic neurons, and all TM clusters were assigned as histaminergic neurons. We identified both glutamatergic and GABAergic clusters in the ARC, DMH, SMN, and PO (fig. S3 and table S10). While these assignments are largely consistent with previous literature (*61*–*63*), rarer populations may not be fully represented in our analysis.

The gene expression signatures of neuronal clusters can be mined for a wealth of information about their marker genes and potential functions. As an example, we considered the distribution of the receptors for neuropeptides involved in the regulation of appetite and satiety, including *LEPR*, *MC4R*, *GHSR*, and *GLP1R*. *LEPR* expression was present across the hypothalamus while being most prominent in the ARC, TM, and DMH. *MC4R* was detected in the PVH. *GHSR* was predominantly expressed in the ARC and, to a lesser degree, also in the LH, VMH, and SCN. *GLP1R* expression could be detected in the PVH (figs. S8 and S14). In summary, our data define the diversity of neuronal subtypes in the human hypothalamus in unprecedented detail.

Maturational trajectories of neurons in the prenatal and adult hypothalamus

Next, we sought to annotate the prenatal neurons and the maturational lineages connecting these cells to adult neurons. Direct annotation of the prenatal neurons proved difficult because many of these cells do not yet express canonical markers. To overcome this issue, we used *Monocle3* to reconstruct a branching pseudotime trajectory incorporating both the prenatal and adult *STMN2*/*SYT1*$^+$ neurons and intermediate progenitors. The tree was rooted at the earliest time point (GW10; Fig. 2F). We identified branch points where the lineages diverge and "leaves" where the lineages terminate and followed the trajectories of these branches and leaves to generate a lineage tree (Fig. 2G). We overlaid the human adult annotations at their most stable level (H108; Fig. 2G and tables S12 and S13 and S15). A small proportion of cells were not contiguous with the lineage tree, although it was largely annotated as ZI. This location may be due to their prethalamic identity. Prenatal neurons were then annotated on the basis of their coclustering with adult neurons in the lineage tree, and the resulting nuclei assignments were supported by the expression of nuclei-specific marker genes (fig. S8). The highest-order branch points largely distinguish GABAergic versus glutamatergic neurons (fig. S7). At the next level, branches largely aligned with the hypothalamic nuclei (fig. S7). The prenatal cells were predominantly positioned at the top of the trajectory. Adult cells were enriched at the termini for all the branches except one (fig. S7). This prenatal branch was composed primarily of intermediate progenitors (fig. S9). Most branch points were robust across three independent pseudotime lineage reconstructions (figs. S10 to 12). Glutamatergic and GABAergic neurons from the same subregion typically were represented by separate branches in the lineage tree, an effect that was also noted within the UMAP (Fig. 2C).

To better understand the gene expression patterns associated with the neuronal lineages, we calculated 15 gene activity patterns using CoGAPS (fig. S13 and table S16). These patterns delineated gene expression programs shared within the major neuron subtypes. Patterns 1, 4, 5, 9, and and 15 mark GABAergic populations across nuclei. Patterns 7, 8, 10, 11, and 14 mark glutamatergic populations, and three of these patterns specifically dissect maturation across the MN (pattern 14 early, 8 middle, and 11 late). Pattern 2 marks histaminergic neurons within the TM. Each CoGAPS pattern is defined by weighted contributions from all genes (table S16), and the hub genes with the strongest weights can be used to characterize transcriptional differences between neuronal populations. For example, the early, middle, and late stages of maturation for the glutamatergic TM lineage were marked by *LRP1B* and *HS6ST3* (pattern 14 hub genes), *GPC6* and *DPP10* (pattern 8), and *CDH18* and *PRKG1* (pattern 11), respectively. Together, the CoGAPS patterns reinforce our finding that large scale, coordinated gene expression drives the organization of the hypothalamus on a major neuron class level but simultaneously influenced by nuclei of origin.

The lineage tree also provides insights into the maturation of neuropeptide gene expression within neuronal lineages (fig. S14). In the ARC, *POMC* was detected at low levels in the first trimester (GW10) and increased to robust levels by the second trimester. *KISS1* was detected by GW12, and *AGRP* was observed by GW18 (fig. S14). In the PVH, the canonical neuropeptide *TRH* was detected in trimester 1 (GW10) and was robustly expressed by the second trimester. Many other neuropeptides such as *OXT* and *AVP* were not observed until the second trimester (GW16; fig. S14).

The expression of transcription factors (TFs) correlated with the maturation of many lineages (Fig. 2H). We studied an ARC branch describing the maturation of *KISS1*$^+$ neurons in a *POMC*-expressing lineage (*64*). TF and neuropeptide expression along pseudotime identified distinct TFs that precede *POMC* expression (e.g., *SOX3* and *INSM1*), coexpress (e.g., *SIX3* and *RORB*), or turn off before *POMC* expression and coincide with *KISS1* expression (e.g., *ESR1* and *TCF4*). Notably, the histone deacetylase *HDAC9* is coexpressed with *POMC* and is potentially interesting as a lineage-specific epigenetic regulator (Fig. 2H). A similar analysis of the Oxytocin expressing (*OXT*) and Arginine vasopressin expressing (*AVP*) neuron lineages in the PVH identified *ZIC1* and *ZFHX4* as TFs that precede detectable expression of these neuropeptides, with *ZFHX4* expression declining before the onset of detectable *OXT* and *AVP* expression. As expected, the well-established PVH TF *SIM1* became detectable at a similar pseudotime as *OXT* and *AVP* (Fig. 2H). These analyses generate numerous, testable hypotheses about the maturation of hypothalamic neurons and its regulatory mechanisms.

Cross-species comparison of hypothalamic neuronal subtypes in humans and mice

Major classes of hypothalamic neurons are shared in humans and mice, but it is unknown whether there are species differences in more refined neuronal subtypes. We integrated our sc/snRNA-seq data from neurons in the human hypothalamic neurons with existing scRNA-seq from the developing mouse hypothalamus (*10*, *11*) and with HypoMap (*59*), an integrated atlas of neurons in the adult mouse hypothalamus derived from 15 scRNA-seq datasets (*4*–*11*, *58*, *65*–*71*) to create a cross-species atlas of hypothalamic neurons (n = 403,176; Fig. 3A, figs. S15 to S17, and table S17). We obtained robust integration of the human and mouse neurons (Fig. 3A and fig. S15) and cells coclustered within major groups corresponding to GABAergic neurons, glutamatergic neurons, and histaminergic neurons (fig. S15B).

We assessed similarities between neuronal subtypes identified in the mouse versus human hypothalamus using our annotations of 108 human neuronal subtypes (H108) and HypoMap's annotation of 129 mouse neuronal subtypes (C185; Fig. 3D and table S18). Clusters were compared on the basis of correlations of marker genes using MetaNeighbor. This approach avoids artifacts associated with integrating cross-species datasets and is conservative in that it keeps the two datasets completely independent before the comparisons. MetaNeighbor reports the similarity among the marker

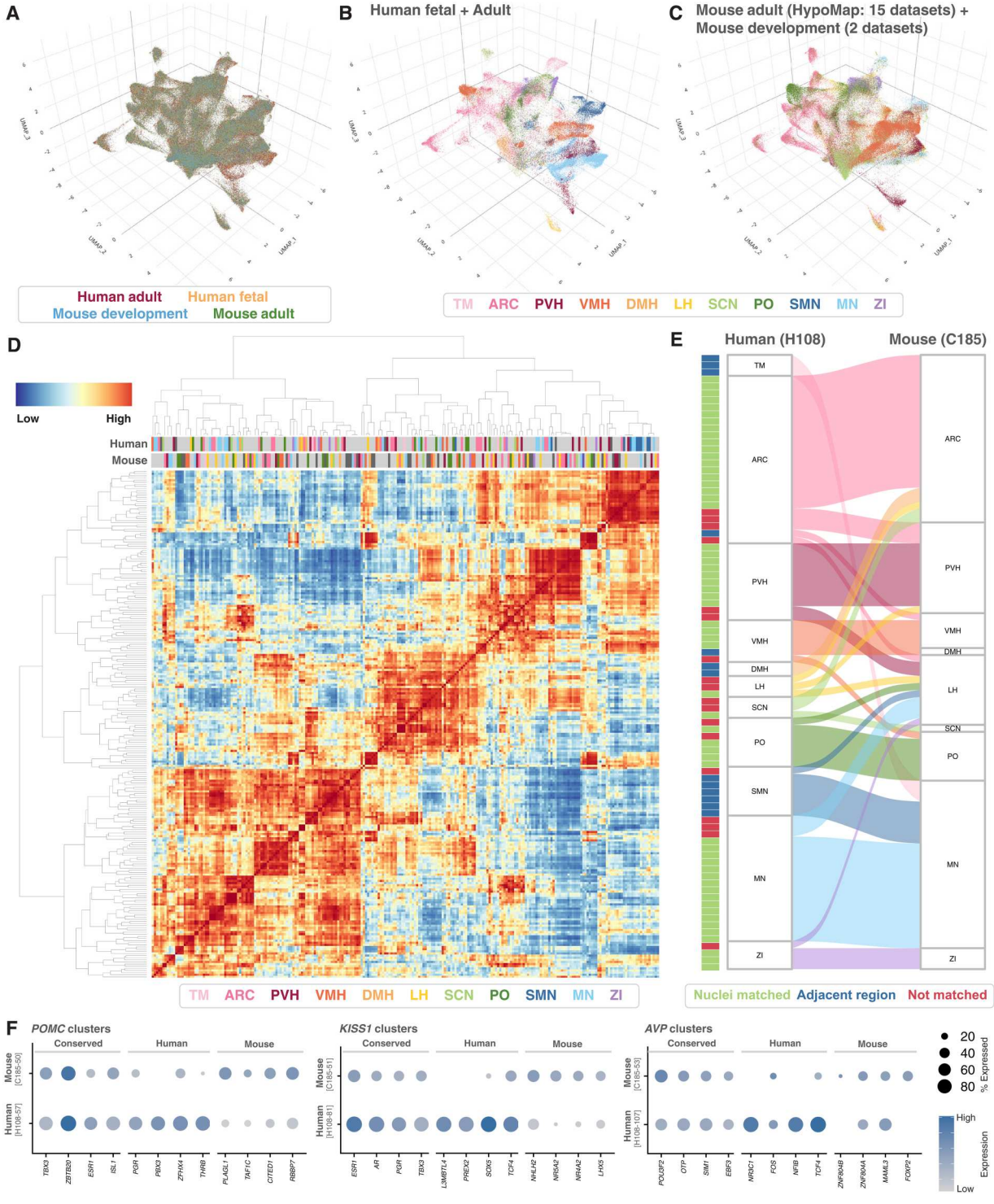

Fig. 3. Cross-species comparison of mouse and human hypothalamic neurons. (**A**) UMAP of single-cell RNA-seq data from the human and mouse hypothalamus neurons, including prenatal and adult samples from 17 additional datasets. Adult mouse data were sourced from HypoMap (*59*) (itself containing 15 datasets), with mouse developmental datasets from Kim *et al.* (*11*) and Romanov *et al.* (*10*), split by species and age (3D UMAP; https://tinyurl.com/2jfprezr). (**B**) Nuclei annotations from the human data (B) and HypoMap annotations (**C**). Nuclei included the TM, ARC, PVH, VMH, DMH, LH, SCN, SMN, MN, PO, and the ZI. (**D**) MetaNeighbor package was used to compare cell-type gene expression profiles for human adult (H108 level) and HypoMap annotations (129 neuronal clusters from the C185 level). (**E**) One hundred five of the 108 clusters at H108 had area under the receiver operator curve (AUROC) score of 0.8 or greater. The majority of the 88 positively identified matches corresponded to clusters with the same nuclei annotations, with a small number of matches annotated to an adjacent nucleus. (**F**) Differential TF expression shows conserved and species enriched TFs for the *POMC*, *KISS1*, and *AVP* clusters.

genes for each pair of clusters as the area under the receiver operator curve (AUROC) and then constructs a hierarchical tree across all the clusters (Fig. 3D). One hundred five of the 108 human clusters (97%) matched a cluster from HypoMap with AUROC > 0.8. This result suggests a very high level of reproducibility across datasets and evolutionary conservation for most neuronal subtypes.

Analyses of the cognate neuronal clusters in the human and mouse hypothalamus also provided a measure of validation for the subregion annotations in both datasets. Whereas our subregion annotations were based primarily on established marker genes, HypoMap is derived from scRNA-seq of microdissected hypothalamic subregions and the subregion annotations were based primarily on this information. We note that both marker genes and microdissection can be imprecise but with relatively independent errors. Eighty-eight of the 108 human neuron clusters had both a predicted subregion localization in our primary analysis and a cognate mouse cluster with a predicted subregion localization. For 58 of these 88 clusters (66%), the cognate mouse cluster was annotated to the same nucleus (Fig. 3E and table S16). For an additional 14 human clusters (16%), the cognate mouse cluster was annotated to an adjacent nucleus. We believe that in many of these cases, the human annotation is correct and the mouse annotation was thrown off by imprecision in the dissections. For 16 human clusters (18%), the mouse and human annotations are mismatched. Thus, by this approach, we were able to validate the subregion localization for up to 69 human neuron clusters, while other annotations both in our dataset and in HypoMap require further validation.

Our discovery of putative homologs for 105 subtypes of mouse and human neurons enabled us to test for shared versus species-specific marker TFs. We calculated differential expression, accounting for differences in sequencing depth and other potential batch effects, to identify both shared and species-specific marker genes within each neuronal subtype. We focused on TFs because these are likely to play an outside role in the regulation of cellular identity and function (table S19). For example, in *POMC*$^+$ clusters, we found that established arcuate TFs including *TBX3* and *ISL1* were conserved markers in both mouse and human. We observed human-enriched expression of *PGR*, *PBX3*, *ZFHX4*, and *THRB* and mouse-enriched expression of *PLAGL1*, *TAF1C*, *CITED1*, and *RBBP7* (Fig. 3F). We performed similar analyses on the *KISS1*$^+$ clusters, where we noted that *TBX3* was also conserved between species. In *AVP*$^+$ clusters, the well-established PVH marker genes *POU3F2*, *OTP*, and *SIM1* were conserved (Fig. 3F), while *NR3C1*, *NFIB*, and *TCF4* were predominantly human and *ZNF804B*, *ZNF804A*, *MAML3*, and *FOXP2* were enriched in mice. Thus, differential expression analysis suggests that there are meaningful differences in the gene regulatory networks (GRNs) active in matched human and mouse neuronal subtypes.

Unique and shared features of hypothalamic versus cortical germinal zones in the human forebrain

Little is known about the genes and trajectories distinguishing neurogenesis in the hypothalamus versus other forebrain regions. It is of particular interest to understand how progenitor populations, despite a common origin, can differ in their gene regulatory programs across brain regions to give rise to all of the specialized cell types unique to specific brain regions. The availability of matched scRNA-seq from the cortex, ganglionic eminence (GE) (the source of telencephalic inhibitory neurons), and hypothalamus from the same fetuses at GW18, GW19, and GW20 provide a unique opportunity to identify shared and region-specific aspects of human neural and glial development. We co-embedded these samples in a shared low-dimensional space, enabling direct comparisons among the progenitor populations and excitatory and inhibitory neuron lineages (n = 95,107; Fig. 4, A and B; fig. S18, A and B; and tables S20 to S22). Both neuronal and non-neuronal lineages emanated from a large cluster of radial glia and were abundantly represented in all three stem cell niches. Radial glia give rise to multiple neuronal and numerous non-neuronal progenitor populations. Of these, among the non-neuronal populations, we identified tanycytes and ependymal cells that were specific to the hypothalamus, as well as astrocytes and oligodendrocytes that were abundant in both the hypothalamus and cortex. A large population of dividing progenitor cells formed a distinct barrel shape in three-dimensional (3D) UMAP space indicative of actively cycling cells [cell cycle stage (fig. S18C) and Seurat clusters 6, 9, and 10 (fig. S18D)]. These dividing progenitors, along with the radial glia, feed into a neuronal lineage that split between excitatory (glutaminergic, *SLC17A6*$^+$) and inhibitory (GABAergic, *SLC32A1*$^+$) lineages and further subdivided into major neuron subclasses. While cortex and GE samples split midway along the developmental lineage between progenitors and mature neuron populations in a largely expected way, we took a keen interest in similarities and differences among these lineages and how progenitors from the hypothalamus fit into this framework.

The co-embedded neurogenic map retains well-known features of cortical neurogenesis. Excitatory neurons of the cortex branched off from inhibitory neurons about halfway along the bridge from early neuron progenitors into mature neuron populations. This lineage led directly into intratelencephalic (IT) excitatory neuron populations and reflected the temporal ordering with which deep layer versus superficial layer IT neurons are born: Newborn neurons at the beginning of the lineage proximal to progenitor cells primarily expressed markers for later-born superficial layer excitatory neurons such as *CUX2*, while more mature neurons at the lineage terminus primarily expressed markers of earlier-born deep layer 5/6 neurons such as *RORB*. A distinct branch in the trajectory expressed markers of extratelencephalic (ET) excitatory neurons. Separately, inhibitory neuron lineages led into three distinct inhibitory neuron clusters, which expressed markers of medial ganglionic eminence-derived (*LHX6*$^+$), caudal ganglionic eminence-derived (*CALB2*$^+$), and lateral ganglionic eminence-derived (*FOXP1*$^+$) subpopulations.

The hypothalamic germinal zone is distinct from germinal zones of the cortex and GE in that it gives rise to both excitatory and inhibitory neurons, and these locally born neurons represent most of the mature neurons within the hypothalamus. Most of the hypothalamic cells were distributed among excitatory and inhibitory lineages that also included cortical and GE-derived cells. This suggests that at a high level of organization the development of excitatory versus inhibitory neurons in the hypothalamus involves shared regulatory programs with the development of excitatory versus inhibitory lineages in the cortex and GE.

The high-level similarity of the developmental trajectories in the cortex, GE, and hypothalamus enabled direct comparisons of the lineages to reveal finer-scale distinctions. Region-specific gene expression differences were already apparent at early stages of

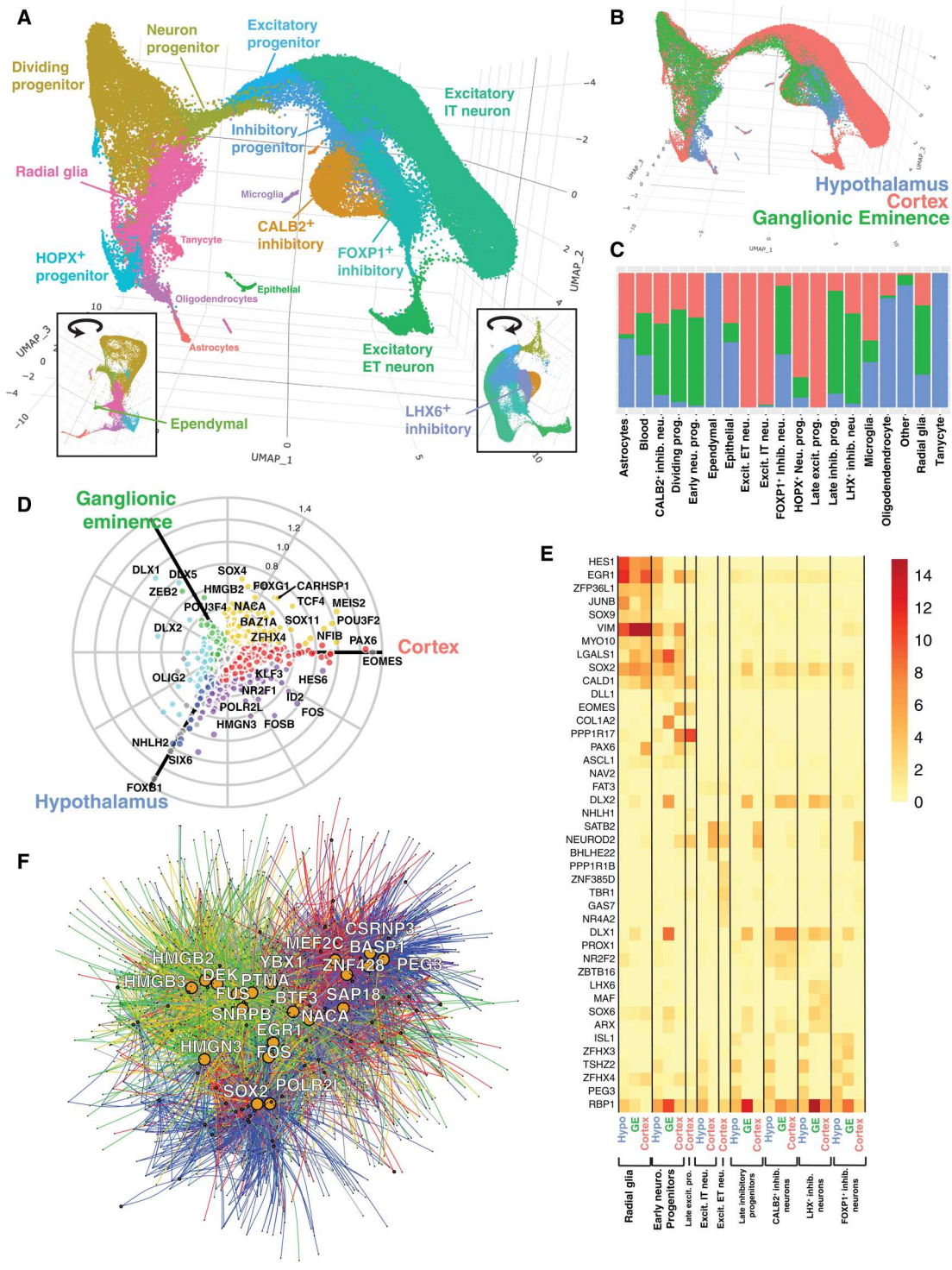

Fig. 4. Developmental principles across distinct human brain regions. (**A**) scRNAseq data from hypothalamus, cortex, and ganglionic eminence for three matched human embryonic samples at GW18, GW19, and GW20. Cell types presented in 3D UMAP (https://tinyurl.com/2p9yzw5h), inset panels are rotations of UMAP showing additional clusters. (**B**) 3D UMAP (https://tinyurl.com/3yazd898) showing overlay of samples by brain region. (**C**) Distribution of cells within cell-type cluster by brain region. (**D**) Polar plot of TF expression across three brain regions for dividing progenitor cells. Points off-axis reflect shared expression between regions. Gray points indicate no significant difference between regions. (**E**) Heatmap depicting genes with similar or divergent expression patterns across neuronal lineages. Colors represent scaled expression of cells only within a given cell-type and brain region, as described in x-axis legend. (**F**) Subsets of GRNs for hypothalamus, cortex, and ganglionic eminence were created on the basis of genes expressed in neural progenitor cells, radial glia, and dividing progenitors. Resulting overlapping networks show edges from hypothalamus network (blue) are roughly evenly split and adjacent to the ganglionic eminence network (green) and cortex network (red). Shared edges follow the color scheme introduced in (D). Top 20 TFs with the greatest number of connections are highlighted in white.

development. In radial glia and actively dividing progenitor populations (clusters 4, 6, 9, and 10 of fig. S18D), we found region-specific elevated expression for developmental TFs such as *PAX6* and *POU3F2* in the cortex, *DLX1* and *DLX5* in the GE (notably *DLX5* expression elevated in CGE), and *FOXB1* and *SIX6* in hypothalamus (Fig. 4D and tables S22 to S24). We also identified shared regulators, including *HES1* and *EGR1* (Fig. 4E). At a later stage of development, in neural progenitors (cluster 11 of fig. S18D), we found increased expression in the hypothalamus for the TF *TSHZ2*, which remained elevated in mature neuron populations. Transcripts with elevated expression in GE neural progenitors included *COL1A2*, a collagen, along with the NOTCH signaling ligand *DLL1* and the cell-cell signaling mediator *LGALS1*. We confirmed cortex-specific expression for canonical progenitor marker genes such as *EOMES*. Many other genes showed complex spatiotemporal patterns in neural progenitors. For instance, neural progenitors of the hypothalamus and cortex had high expression (compared to GE) for cytoskeletal proteins such as *MYO10*, *CALD1*, and *VIM*, whereas neural progenitors in the hypothalamus and GE (but not cortex) had shared expression of *RBP1* involved in retinoic acid signaling (*72*). Other genes had different temporal patterns or different cell-type specificity. For example, *PPP1R17*, a phosphatase regulatory subunit, was identified as a neural progenitor marker within the cortex, where the expression increases throughout neural maturation (*57*). However, in the hypothalamus, *PPP1R17* is instead expressed most highly in radial glia, with expression concentrated in the DMH. Genes that exhibited a similar enrichment in hypothalamic radial glia but later enrichment in mature cortex populations include *FAT3*, a cadherin involved in dendrite development and neuron migration, and the helicase *NAV2*, a member of the neuron navigator gene family involved in neuron growth and migration. These results provide insight into the unique regulatory programs that give rise to specialized neuronal populations.

We applied a gene network approach to gain further insight into the shared versus unique drivers of neuronal development across lineages. Gene coexpression network modeling identified 28 gene coexpression modules, many of which were expressed in region- and stage-specific patterns across the development of excitatory and inhibitory neuronal lineages (fig. S18E and tables S25 to S27). In addition, we reconstructed a GRN model (*73*) to predict the target genes for 1317 TFs in each germinal zone and the key regulator TFs for each gene coexpression module. We found both region-specific and shared TF-gene associations, where the extent of overlap across models provides a measure for the rewiring of these networks across brain regions. We illustrate this concept for the 20 most highly connected "hub" TFs (Fig. 4F). For these TFs, we detect many TF-gene edges that are reproducible within different samples from the same brain region but not across brain regions, suggesting substantial rewiring. Network edges detected in the hypothalamus appear to be split between cortical and GE-derived groups, suggesting an early lineage difference not distinguished in the UMAP in Fig. 4A. Gene network modeling also provided insights into the regulation of specific neuronal lineages. The gene coexpression module M73 (fig. S18E) was expressed across the entire excitatory neuron lineage from dividing progenitor cells to mature neurons, enabling us to compare the regulators of excitatory neuron development across regions. Several TFs were identified as key regulators of excitatory neuron development in both hypothalamus and cortex, including *NEUROD6*, *ANK2*, *MYT1L*, and *CSRNP3*. Strikingly, we also identified region-specific regulators of excitatory neurons, including hypothalamus-enriched (e.g., *CSRNP3*, *ARID4A*, *PEG3*, and *BASP1*) and cortex-enriched TFs (*MEF2C*, *ZBTB18*, and *SATB2*). Similarly, module M70 was expressed across the entire inhibitory lineage, and we used this module to compare the regulators of inhibitory lineages in hypothalamus and GE (fig. S18E). We identified *SP9*, *DLX5*, *DLX2*, *SOX11*, and *SOX4* as shared regulators of inhibitory neuron development across regions, in addition to hypothalamus-enriched (*SCAND1*, *ZNF428*, *YBX1*, and *PTMA*) and GE-enriched TFs (*CITED2*, *TCF4*, *LHX6*, and *ARX*). This same pattern of shared and region-enriched regulators could be identified in several additional modules, including M42, which is activated at later stages of excitatory neuron development (fig. S18E). These results suggest that there are shared "core" regulatory programs that govern the development of excitatory and inhibitory neurons in multiple brain regions, which may be refined by region-specific regulatory programs that give rise to the unique properties of each region's excitatory and inhibitory populations.

DISCUSSION

Here, we have described the development and diversity of neuronal and non-neuronal cell types of the human hypothalamus from prenatal stages to adulthood at single-cell resolution. We identified 108 robust neuronal subtypes in the adult hypothalamus and provided evidence for up to 369 transcriptionally distinct neuronal clusters. Reconstruction of a lineage tree enabled us to annotate prenatal neurons and the gene expression changes that occur during their maturation. Cross-species comparisons revealed a remarkable degree of conservation, with 105 of 108 human neuron subtypes having a cognate subtype identified in mice. Comparisons of neurogenic and gliogenic trajectories in hypothalamus versus other forebrain regions identified both shared and hypothalamus-specific aspects of neurodevelopment. Together, these data resources and analyses provide an unprecedented depth of information about the cell types in the human hypothalamus.

Within our prenatal samples, we observe sequential formation of all cell types expected within the hypothalamus. These originate from several progenitor populations that resemble those described previously (*16*, *47*, *53*). On the basis of the gene expression profile, our qRGC cluster is analogous to the homonymous cluster in Zhang *et al.* (*47*), the clusters HPC_1-3 and HPC_1-4 reported in Zhou *et al.* (*53*). These cells likely represent the RG populations that line the ventricle. Our cRGC cluster also represents an analogous population to that reported in Zhang *et al.* (*47*), and the HPC_1-1 cluster reported by Zhou *et al.* (*53*) These proliferative cells are akin to the migratory mantle radial glia. A third radial glia cluster, tRGCs, appear similar to the HPC_1-2 cluster reported by Zhou *et al.* (*53*) and represents a progenitor population primed for lineage specification.

We also note three intermediate progenitor populations including two *ASCL1*$^+$ populations and one *NEUROD2*$^+$ population similar to those reported previously by Zhang *et al.* (*16*, *47*). In Zhou *et al.* (*53*), this gene expression is akin to HPC_2, HPC_3, and HPC_5, respectively (*53*). One *ASCL1* cluster and the *NEUROD2*$^+$ cluster (IPC_2/3) each expressed neuronal markers *STMN2/SYT1*, suggesting that they were lineage specified.

Within our pseudotime trajectory, these were localized together between GABAergic and glutamatergic neurons. In contrast, the *ASCL1*$^{+}$*STMN2*$^{-}$/*SYT1*$^{-}$ cluster (IPC_1) expressed gliogenic markers including *OLIG1*, *OLIG2*, and *EGFR*, suggesting that these are precursors to astrocytes or oligodendrocytes (*74*–*77*).

Our analysis provides substantial insights into neuronal diversity in the adult hypothalamus. At the most stable clustering resolution, we characterized 108 neuronal subtypes and we found evidence for up to 369 transcriptionally distinct neuronal clusters. More than 90% of these clusters could be annotated to specific hypothalamic nuclei based on their marker genes. The number of neuronal subtypes is comparable to the number of subtypes detected by scRNA-seq in mice (*59*). Recent spatial transcriptomics from the mouse brain suggests that the actual number of cell populations in the hypothalamus may be even larger (*78*). Our atlas describes more than three times the number of distinct populations described previously for the human hypothalamus (*52*). The increased resolution of our dataset can be attributed to adult time points with more mature neurons. However, we expect more subtypes to emerge with more detailed sequencing and the inclusion of samples from female donors to identify cell populations that are sexually dimorphic.

Our pseudotime lineage tree provides insights into the transcriptional similarities and differences among hypothalamic neurons during their prenatal maturation. We observe that fate-committed neurons are distinguished both by their neurotransmitter class and by their subregion. Our analysis is consistent with a sequential specification of hypothalamic neurons, expanding on prior literature (*4*–*11*, *52*, *59*, *65*–*71*, *79*). Early in hypothalamic development, developing neurons attain a unique transcriptional identity corresponding to the nucleus in which they reside. Later, specific neuronal subtypes differentiate. This process was well underway by 10 weeks of gestational age, at which time we were able to discern most nuclei by the expression of established markers.

Neurons within the hypothalamus have dual identities on the basis of the neurotransmitters and neuropeptides they use, as well as by their subregion localization. While arealization of other brain regions such as the cortex and cerebellum involves subtle, quantitative differences within the same neuronal subclasses, in the hypothalamus, each subregion has its own distinctive types of neurons. Thus, it may come as a surprise that both in our clustering of adult neurons and in our lineage tree for neuronal maturation trajectories, much of the clustering is driven by neurotransmitter class (GABAergic versus glutamatergic neurons). We believe that this reflects that the gene regulatory programs to produce these major classes of neurons involve many neurotransmitter class-related genes that are shared across nuclei. In addition, in many nuclei, most or all of the neurons are of the same neurotransmitter class. For instance, the LH, VMH, PVH, and MN clusters all expressed glutaminergic markers. This has been previously reported in mouse single-cell data from the VMH (*7*, *65*, *80*), MN (*68*), and PVH (*81*), but previous observations in mice suggest that we may be missing mixed neuronal populations within the LH (*8*). This may have occurred due to conservative dissection favoring the more medial regions. This may also explain the relative underrepresentation of LH neurons compared to other nuclei. The SCN and ZI clusters all expressed GABAergic markers in line with the previous reports in the mouse SCN (*67*). The TM contains exclusively histaminergic neurons (*82*). The ARC, DMH, PO, and SMN contained mixed glutamatergic and GABAergic populations, as has been reported previously in the ARC (*80*) and the PO (*6*). However, in rats, the ARC and DMH are predominantly GABAergic (*61*–*63*), so there may be species-specific aspects in neurocircuitry.

These resources will provide detailed information about the cell types involved in many hypothalamic functions. Focusing on the roles of the hypothalamus in energy homeostasis, we studied the distribution of the hormone receptors *LEPR* and *GHSR* in the adult arcuate. While we confirm the existence of *POMC/LEPR*$^{+}$cells in humans as have been described in mice, we did not detect a *POMC/GLP1R*$^{+}$ population as established in mice (*83*). We detected substantial *GLP1R* expression in the PVH. This suggests several possible scenarios: (i) A potential human *POMC/GLP1R*$^{+}$ population may have low levels of *GLP1R*, which are below the detection threshold for snRNA-seq, (ii) our sampling strategies were not successful in including this populations, or (iii) albeit unlikely, this population is not present in humans. Further studies are needed to explore these subpopulations in detail. As known from mice, *GHSR* was predominantly expressed in the ARC and, to a lesser degree, also in other hypothalamic regions such as the LH, VMH, and SCN (*43*). As expected, *MC4R* is expressed in the PVH (*84*). None of these receptors showed substantial expression in the prenatal samples. In mice, these receptors are known to be lowly expressed genes with higher expression in the adult as compared to embryonic stages (*43*). Thus, their expression level in the human prenatal hypothalamus might have been too low for reliable detection by single-cell transcriptomics.

In the PVH, we show key TFs such as *SIM1*, *POU3F2*, and *NHLH2* are strongly expressed from GW10. In mice, *Sim1* or *Pou3f2* knockouts are known to result in strong suppression of *Oxt*, *Crh*, *Avp*, and *Trh* neurons (*85*, *86*). Expression of PVH neuropeptides generally did not begin until trimester 2. Our results detect these neuropeptides slightly later than in previous studies where *OXT* has been noted at GW14 and *CRH* and *AVP* as early as GW12 (*49*, *51*, *87*, *88*). The trajectories of neuronal maturation and specification are less well studied in most other nuclei. We expect that these data will be a useful resource for mapping lineages, although not all neuropeptides may be noted due to sample dissection issues (i.e., undersampled arcuate in GW22 and GW25 samples), or that cells are still ongoing differentiation, diversification, and maturation to the various peptidergic subtypes.

As noted above, variation in the prenatal environment can have lasting consequences on many hypothalamic functions (*34*, *35*, *40*, *44*), but it is not well understood why adverse prenatal environments lead to worse or different outcomes in some individuals and not others. Precisely delineating the timing at which hypothalamic nuclei mature could provide insight into these exposures and outcomes, including the possibility that differences in the developmental timing among hypothalamic nuclei could produce distinct sensitive periods within the developmental trajectory and different disease risks.

Mouse models have been used extensively to study the relationships among the prenatal environment, the development of the hypothalamus, and the emergence of behavioral and physiological variation in hypothalamic functions. Thus, a critical question is whether these developmental processes are conserved in mice versus humans. We found a remarkably high degree of evolutionary conservation for neuronal subtypes in mice and humans, with a putative mouse homolog for 105 of the 108 human neuron clusters. Differential expression analyses showed that many TFs have

shared patterns of enrichment across these neuronal subtypes. It is possible that there are human-specific cell populations at more granular levels of resolution, and we do detect what appear to be meaningful differences in TF utilization across species. Nonetheless, the overall conservation of cell types both validates our annotations and bodes well for the translation of findings from mice into humans.

Our comparison of forebrain neurogenic niches revealed shared lineages leading to excitatory and inhibitory neurons in the hypothalamus, cortex, and GE. However, gene expression differences were detectable between regions starting at early stages of development in radial glia. GRN models suggested that the differentiation of excitatory versus inhibitory neurons occurs early in hypothalamic development and involves "core" regulatory programs that are shared, respectively, by excitatory and inhibitory neuronal lineages in the cortex and GE. We present evidence that these core programs are refined by region-specific TFs that may give rise to the unique properties of the excitatory and inhibitory programs in each brain region. While some of these predicted regulators have been described previously (*46*), our models make numerous predictions for the roles of key regulator TFs, and these should be tested experimentally. As some of these networks are predicted to be human specific, testing their functions will likely require the further development of human cell culture systems that enable direct comparisons across forebrain stem cell niches.

Several limitations should be noted. As with most human studies, there was substantial sample-to-sample variability, and we cannot control for inherent variation among individuals. Our dataset lacks samples from the third trimester of gestations and from postnatal developmental time points, and incorporating these samples will be essential to resolve later stages of neuronal maturation. The adult dataset did not include females, so sex differences could not be assessed. While we have taken extensive efforts to validate our cell type annotations and trajectories, these remain bioinformatic predictions. Spatial transcriptomic data and single-cell transcriptomic data from more finely dissected samples are needed to further resolve anatomical nuclei and nuclei subregions, including discovering transcriptomic signatures for poorly annotated nuclei. Last, there was limited information about the prenatal environment experienced by the fetuses that we studied. An exciting future direction will be to expand our analysis to human and model organism samples with known variation in the prenatal environment, enabling a more direct evaluation of sensitive periods and their developmental consequences.

The data presented here represent an important resource for understanding the development and diversity of cell types in the human hypothalamus. We anticipate that these resources will be valuable for many applications, including evaluation of the cell-type distributions for genes involved in the pathophysiology of human diseases. To facilitate the utilization of our data, we have created web resources for the visualization of cell type–specific gene expression at NeMO Analytics (https://nemoanalytics.org/p?l=a856c14e&g=gad2).

MATERIALS AND METHODS

Prenatal sample collection and processing

Acquisition of all primary human tissue samples was approved by the UCSF Human Gamete, Embryo and Stem Cell Research Committee (approval nos. 10-03379 and 10-05113). All experiments were performed in accordance with protocol guidelines. Maternal informed consent was obtained before sample collection and use for this study. First and second trimester human hypothalamus tissue was collected from elective pregnancy termination specimens from San Francisco General Hospital and the Human Developmental Biology Resource (HDBR). Cortical and ganglionic eminence tissue was collected in parallel from the same specimens, as previously described (*56*, *57*). Hypothalamic tissue samples were dissociated using papain (Worthington) containing deoxyribonuclease. Samples were grossly chopped and then placed in 1 ml of papain and incubated at 37°C for 15 min. Samples were inverted three times and continued incubating for another 15 min. Next, samples were triturated by manually pipetting with a glass pasteur pipette approximately 10 times. Dissociated cells were spun down at 300*g* for 5 min, and papain was removed.

Adult sample collection and processing

Hypothalamus tissue from three adults were obtained by the Allen Institute from a 50-year-old male donor (subject ID H18.30.002, right hemisphere, cause of death = cardiovascular, post-mortem interval (PMI) = 10 hours, tissue RNA integrity number (RIN) score = 8.2 ± 0.4), a 42-year-old male donor (subject ID H19.30.001, right hemisphere, cause of death = suicide, PMI = 8 hours, tissue RIN score = 7.91), and a 29-year-old male donor (subject ID H19.30.002, right hemisphere, cause of death = cardiac arrest, PMI = 7.5 hours, tissue RIN score = 8.15) with no exclusionary medical history and negative for infectious disease. Tissue collection was performed in accordance with the provisions of the U.S. Uniform Anatomical Gift Act of 2006 described in the California Health and Safety Code section 7150 (effective 1 January 2008) and other applicable state and federal laws and regulations. The Western Institutional Review Board (IRB) reviewed tissue collection procedures and determined that they did not constitute human subjects research requiring IRB review. The deidentified postmortem brain sample was obtained after receiving permission from the decedent's legal next-of-kin and prepared as described previously (full methods described in (*89*) (dx.doi.org/10.17504/protocols.io.bf4ajqse) and Bakken *et al.* (*90*) describes subject ID H18.30.002 sample and Siletti *et al.* (*91*) describes subject ID's H19.30.001 and H19.30.002. Briefly, coronal brain slabs of 1 cm thickness were frozen in dry ice-cooled isopentane and transferred to vacuum-sealed bags for storage at −80°C until the time of further use. To isolate the brain regions of interest, tissue slabs were briefly transferred to −20°C and the region of interest was removed and subdivided into smaller blocks on a custom temperature controlled cold table. Tissue blocks were stored at −80°C in vacuum-sealed bags until later use. Figure S1 details the four broad regions—preoptic, supraoptic, tuberal, and mammillary, identified by gross anatomical landmarks for the hypothalamus dissections. Nucleus isolation for 10X Chromium Single Cell 3′ RNA sequencing V3 was conducted as described (dx.doi.org/10.17504/protocols.io.y6rfzd6). Gating on 4′,6-diamidino-2-phenylindole and NeuN fluorescence intensity was carried out as described previously (*89*). $NeuN^+$ and $NeuN^-$ nuclei were sorted into separate tubes and were pooled at a defined ratio after sorting. Sorted samples were centrifuged; frozen in a solution of 1× phosphate-buffered saline, 1% bovine serum albumin, 10% dimethyl sulfoxide, and 0.5% RNAsin Plus RNase Inhibitor (Promega, N2611); and stored at

−80°C until the time of shipment on dry ice from the Allen Institute to the Karolinska Institute for 10X chip loading.

Sequencing

For prenatal samples, single-cell capture was performed following the 10X Chromium v2 manufacturer's instructions. Each sample was its own batch. For each batch, 10,000 cells were targeted for capture and 12 cycles of amplification for each of the complementary DNA and library amplifications were performed. Libraries were sequenced according to the manufacturer's instructions on the Illumnia NovaSeq 6000 S2 flow cell (RRID:SCR_016387). For adult samples, immediately before loading on the 10X Chromium instrument, frozen nuclei were thawed at 37°C, washed, and quantified for loading as described (dx.doi.org/10.17504/protocols.io.nx3dfqn). Briefly, suspensions were thawed in a 37°C water bath, spun down briefly, and pipetted several times to mix. Nuclei were then processed according to the 10X Genomics protocol, targeting 5000 cells. All samples were processed with the 10X Genomics V3 kit. Samples were first sequenced to a shallow depth (approximately 1000 reads per cell) on the Illumina NextSeq platform to validate sample concentrations. Samples were then sequenced to approximately 100,000 reads per cell on the Illumina NovaSeq platform. After sequencing, saturation was calculated for each sample using the Preseq package (*92*). Any samples that were not saturated to 60% were sequenced more deeply using Preseq predictions.

Quality filtering and integration

All samples were aligned and preprocessed using cellranger. All prenatal samples were quality filtered to include cells with the number of detected genes between 200 and 4000, a total unique molecular identifiers (UMIs) between 1000 and 15,000, and a maximum 10% of reads mapping to mitochondrial genes. Adult neurons were filtered to include cells with the number of detected genes between 200 and 10,000; a total UMI between 1000 and 100,000; and a maximum 10% of reads mapping to mitochondrial genes. For published datasets, cells passing quality filters defined in publication were used in this study. Doublets were detected using scDblFinder (default parameters, clust.method = "overcluster") and discarded from the analysis. Unless otherwise noted, the Seurat package v4.0.5 (*93*) was used for normalization, sample integration, clustering, differential gene expression analysis, and plotting. Additional visualizations were produced using the plotly package (v4.10.2), ggplot2 (v3.4.2), igraph (v1.5.0), and ggalluvial (v0.12.5).

Cell-type assignments

Integrated prenatal samples (n cells = 155,183) were subject to dimension reduction with principal components analysis (PCA) and were visualized in the 3D UMAP space. Cells were clustered using Louvain clustering and identified using established markers from published studies (*2*, *4*–*11*, *23*, *58*, *76*, *94*–*96*). Aberrant cells were manually reassigned on the basis of UMAP coordinates to best reflect gene expression in feature plots. Extrahypothalamic cells such as *FOXG1*$^+$ cells (telencephalon) and *NEUROD6*$^+$ cells (forebrain) were removed prior downstream analysis. For the adult sample, extrahypothalamic cells such as *PPP1R1B*/*DRD1*/*PDYN*/*DRD2*/*ADORA2A*$^+$ cells (Nucleus accumbens) were removed from the anterior samples (preoptic and supraoptic) prior downstream analysis.

Iterative clustering

Seurat clustering was used to generate neuronal clusters at 15 levels of resolution from the adult hypothalamic neurons. These 15 levels of resolution were integrated into a single hierarchical tree using the mrtree package (v0.0.0.9000, default parameters) (*97*). This tree was further refined by merging branches that exhibited sample bias (greater than 80% of cells from a single sample) or did not produce at least 10 differentially expressed genes (excluding mitochondrial (MT) and ribosomal genes) with a minimum log fold change of 0.5 and an adjusted P value greater 0.05. Nuclei annotations were performed at the H6, H55, H108, and H369 levels based on expression of marker genes for each nuclei based on previously published studies (table S3) and/or localization in the Allen Brain Atlas (figs. S4 and S6) (*60*) or the Human Protein Atlas (*98*). Nuclei assignments also took into consideration the region of dissection and—after integration with HypoMap—whether the clusters had strong alignment with a region-specific dataset.

Cluster robustness

Cluster robustness was assessed using methodology and individual functions from the chooseR package (*99*). One hundred iterations of cluster generation was performed as described above (Seurat clustering at 15 resolutions followed by mrtree), where each iteration used a random sampling of 80% of the original cells in the human adult neuron dataset. Silhouette scores for each cell were calculated from a distance matrix defined by 1 − frequency value of coclustering, and average silhouette scores per cluster were presented and 95% confidence intervals were calculated using the boot_median function from chooseR.

Nuclei assessment based on Allen ISH data

Cluster annotation was double checked against mouse in situ hybridization (ISH) data available from the Allen institute. Functions from the scCoco package (v0.0.0.9000; https://github.com/lsteuernagel/scCoco), which, in turn, is a wrapper for functions in the cocoframer (v0.1.1) (*60*), were used in R to assess likely nuclei assignments based on clustering of human data. To be comparable to HypoMap, marker gene lists were identified by running FindAllMarkers on per H53 cluster using genes included in the Allen Mouse Brain Atlas ISH database (*60*). Top significantly expressed marker genes per H53 cluster were entered into the findRegions_genesets function (parameters target_structure_id = "1097", exclude_ids = c("338"), target_level = "8") to identify likely nuclei per cluster.

Neuronal lineage analysis

Prenatal and adult hypothalamic neurons (CS22-Adult; n = 121,821) were integrated. Seurat was then used for dimension reduction using PCA and generation of a 3D UMAP. Monocle3 (*100*) was used to generate pseudotime lineages encompassing both prenatal and adult neurons. The Monocle3 trajectory generated 514 vertices. Vertex Y_376 was chosen as the starting node as it contained the highest proportion of the earliest time point—GW10 (66%). Three additional lineages were generated to show robustness: Alternative lineage #1 was generated with the k-parameter reduced from 100 to 20 (992 nodes with Y-137 as the starting node). Alternative lineage #2 was generated with the k-parameter increased from 100 to 150 (394 nodes with Y-26 as the starting node). Alternative lineage #3 was generated with the spread parameter increased

from 3 to 6 (399 nodes with Y-31 as the starting node). Using these pseudotime lineages, we identified branch points where the lineages diverge and leaves where the lineages terminate. Using the all_simple_paths function in Monocle3 and the igraph package, we were able to generate 2D lineage trees to represent each of the cells along the pseudotime trajectory. Nuclei annotations from the H108 level were overlaid onto the main pseudotime trajectory, and prenatal nuclei annotations were extrapolated to the adult nuclei annotation if the vertex contained either (i) less than 60% prenatal cells and more than 20% of adult cells with the dominant nuclei annotation or (ii) less than 80% prenatal cells but the remaining adult cells were composed of less than two nuclei. Neurotransmitter classes were extrapolated if a vertex contained less than 75% prenatal cells but contained more than 40% of adult cells assigned to the dominant neurotransmitter. In addition, gene expression was overlaid onto these lineage trees, which showed the cells organizing into distinct neurotransmitter classes and further branching to form branches representing 11 anatomically distinct regions (fig. S7). To identify which TFs modulate their activity in distinct branches, we used the Monocle3 function fit_models and plotted the top 20 to 25 TF′s by descending q value that correlates with pseudotime along the branch. CoGAPS patterns in the human neuron dataset were identified using the CoGAPS package (v3.14.0) (*101*) in R. Default parameters were used for the CoGAPS function except nPatterns = 15 and nIterations = 10,000.

Comparison across human/mouse and adult/prenatal neurons

Human adult hypothalamic neurons (n = 85,913) and human prenatal neurons (n = 35,908) were integrated with mouse developmental samples (n = 60,684) from Kim *et al.* (*11*) and (n = 34,324) from Romanov *et al.* (*10*) and mouse adult data sourced from HypoMap (n = 186,374), composing of n = 16,043 from a VMH dissection from Affinati *et al.* (*65*); n = 20,766 from the VMH dissection from Kim *et al.* (*7*); n = 17,969 from the VMH dissection from Liu *et al.* (*66*); n = 12,822 from the ARC dissection from Campbell *et al.* (*4*); n = 17,693 from the PO dissection from Moffitt *et al.* (*6*); n = 23,817 from the SCN dissection from Morris *et al.* (*67*); n = 13,756 from the SCN dissection from Wen *et al.* (*9*); n = 5391 from the LH dissection from Rossi *et al.* (*69*); n = 4573 from the LH dissection from Mickelsen *et al.* (*8*); n = 9215 from the ventral posterior hypothalamus dissection from Mickelsen *et al.* (*68*); n = 23,667 sorted Lepr$^+$ cells from Rupp *et al.* (*70*); n = 14,434 from the whole hypothalamus from Zeisel *et al.* (*58*); n = 5272 from the whole hypothalamus from Chen *et al.* (*5*); and n = 929 from the whole hypothalamus from Lee *et al.* (*71*). Cells passing quality filters defined in publication were used in this study. Before integration, mouse genes names were converted to human format using the ConvertGeneNames from the Azimuth package (v0.4.6). Normalization and dimension reduction were performed as described previously, and samples were integrated using reciprocal PCA.

The MetaNeighbor (v1.12.0) function MetaNeighborUS (fast_version = TRUE) was used to compare our clusters at the H108 level to the 129 neuronal clusters from HypoMap at the C185 level (*102*). Reciprocal clustered were defined as the cluster pairing with an AUROC > 0.8 with the highest cluster selected if required. The respective nuclei annotations were compared, and the pairs that were annotated to MN/SMN, MN/TM, ARC/VMH, DMH/VMH, LH/SMN, LH/ZI, or LH/PO were indicated as adjacent nuclei based on localization within both the human and mouse in the Allen Brain Atlas (*60*).

To compare these reciprocal clusters at the gene level, we regressed out the number of UMI and performed differential gene expression on the common TFs across both the mouse and human adult datasets using the FindAllMarkers function from Seurat. We then compared TFs with a $P < 0.05$ and a $\log_2$ fold change > 0.5 across each of the reciprocal pairs. TFs that were common to both were denoted as "conserved," with the remaining indicated to be enriched in either mouse or human.

Comparison across brain regions during human development

Three fetuses from GW18, GW19, and GW20 were chosen for their broad range of dissections covering the hypothalamus, three regions of the ganglionic eminence, and five regions of the cortex. Adult neurons were filtered to include cells with at least 1000 reads (maximum 15,000), number of genes 500 to 4000, a maximum 10% of reads mapping to mitochondrial genes, and total UMI above 1000. The 95,107 cells passing these filters were integrated using the Seurat package in R with the same parameters as used for other datasets in this study. Cell-type assignments were determined by a mixture of our work with the hypothalamus and cortex assignments previously reported (*96*). Three dimensional UMAP projections assisted in identification of multiple excitatory and inhibitory lineages as well as distinguishing ET and IT excitatory neurons and the three inhibitory neuron populations. Identification of IT and ET neuron types were further confirmed using projectR package (*103*) and the DeCoN dataset (*104*). Seurat clustering at a resolution of 0.5 largely delineated major cell types. The Seurat function FindAllMarkers was used to both find top marker genes for each Seurat cluster and identifying brain region differences among Seurat clusters. Polar coordinate plots and z scores were calculated using the volcano3D (v2.0.1) package (*105*) and were used to identify top TF differences among dividing progenitor cells. Genes selected for the heatmap in Fig. 4E were a combination of top marker genes per Seurat cluster that were both either similar or different across brain regions. GRNs were reconstructed using the Genie3 package (v1.16.0) (*73*). Networks were first built for each individual sample, and then edge weights were averaged across samples to identify region-specific networks. For summary analysis of networks in dividing cells, networks were combined by finding common edges and the resulting network was plotted using the iGraph package (v. 1.2.6). TFs with the greatest number of connections were displayed in white in Fig. 4F. Gene modules were created using k-means clustering starting with a k = 100 and resulting in 28 groups, with gene eigenvalues calculated with the WGCNA package (*106*). Counts tables for both Genie3 and k-means clustering analysis were imputed using k-nearest neighbors smoothing, where k = 5. We then compared GRNs across brain regions to identify region-specific TF drivers for each gene module. TFs with poor correlation between the TF expression and the gene module eigenvalue were discarded. Lists of TF drivers per gene module word compared across brain regions and similarities and differences can be found in the supplementary tables.

Supplementary Materials

This PDF file includes:
Figs. S1 to S18
Legends for tables S1 to S27

Other Supplementary Material for this manuscript includes the following:
Tables S1 to S27

REFERENCES AND NOTES

1. Y. Xie, R. I. Dorsky, Development of the hypothalamus: Conservation, modification and innovation. *Development* **144**, 1588–1599 (2017).
2. J. L. Bedont, E. A. Newman, S. Blackshaw, Patterning, specification, and differentiation in the developing hypothalamus. *Wiley Interdiscip. Rev. Dev. Biol.* **4**, 445–468 (2015).
3. C. B. Saper, B. B. Lowell, The hypothalamus. *Curr. Biol.* **24**, R1111–R1116 (2014).
4. J. N. Campbell, E. Z. Macosko, H. Fenselau, T. H. Pers, A. Lyubetskaya, D. Tenen, M. Goldman, A. M. J. Verstegen, J. M. Resch, S. A. McCarroll, E. D. Rosen, B. B. Lowell, L. T. Tsai, A molecular census of arcuate hypothalamus and median eminence cell types. *Nat. Neurosci.* **20**, 484–496 (2017).
5. R. Chen, X. Wu, L. Jiang, Y. Zhang, Single-cell RNA-seq reveals hypothalamic cell diversity. *Cell Rep.* **18**, 3227–3241 (2017).
6. J. R. Moffitt, D. Bambah-Mukku, S. W. Eichhorn, E. Vaughn, K. Shekhar, J. D. Perez, N. D. Rubinstein, J. Hao, A. Regev, C. Dulac, X. Zhuang, Molecular, spatial, and functional single-cell profiling of the hypothalamic preoptic region. *Science* **362**, eaau5324 (2018).
7. D. W. Kim, Z. Yao, L. T. Graybuck, T. K. Kim, T. N. Nguyen, K. A. Smith, O. Fong, L. Yi, N. Koulena, N. Pierson, S. Shah, L. Lo, A. H. Pool, Y. Oka, L. Pachter, L. Cai, B. Tasic, H. Zeng, D. J. Anderson, Multimodal analysis of cell types in a hypothalamic node controlling social behavior. *Cell* **179**, 713–728.e17 (2019).
8. L. E. Mickelsen, M. Bolisetty, B. R. Chimileski, A. Fujita, E. J. Beltrami, J. T. Costanzo, J. R. Naparstek, P. Robson, A. C. Jackson, Single-cell transcriptomic analysis of the lateral hypothalamic area reveals molecularly distinct populations of inhibitory and excitatory neurons. *Nat. Neurosci.* **22**, 642–656 (2019).
9. S. Wen, D. Ma, M. Zhao, L. Xie, Q. Wu, L. Gou, C. Zhu, Y. Fan, H. Wang, J. Yan, Spatiotemporal single-cell analysis of gene expression in the mouse suprachiasmatic nucleus. *Nat. Neurosci.* **23**, 456–467 (2020).
10. R. A. Romanov, E. O. Tretiakov, M. E. Kastriti, M. Zupancic, M. Häring, S. Korchynska, K. Popadin, M. Benevento, P. Rebernik, F. Lallemend, K. Nishimori, F. Clotman, W. D. Andrews, J. G. Parnavelas, M. Farlik, C. Bock, I. Adameyko, T. Hökfelt, E. Keimpema, T. Harkany, Molecular design of hypothalamus development. *Nature* **582**, 246–252 (2020).
11. D. W. Kim, P. W. Washington, Z. Q. Wang, S. H. Lin, C. Sun, B. T. Ismail, H. Wang, L. Jiang, S. Blackshaw, The cellular and molecular landscape of hypothalamic patterning and differentiation from embryonic to late postnatal development. *Nat. Commun.* **11**, 4360 (2020).
12. L. W. Swanson, G. Sanchez-Watts, A. G. Watts, Comparison of melanin-concentrating hormone and hypocretin/orexin mRNA expression patterns in a new parceling scheme of the lateral hypothalamic zone. *Neurosci. Lett.* **387**, 80–84 (2005).
13. D. M. Simmons, L. W. Swanson, High-resolution paraventricular nucleus serial section model constructed within a traditional rat brain atlas. *Neurosci. Lett.* **438**, 85–89 (2008).
14. D. M. Simmons, L. W. Swanson, Comparison of the spatial distribution of seven types of neuroendocrine neurons in the rat paraventricular nucleus: Toward a global 3D model. *J. Comp. Neurol.* **516**, 423–441 (2009).
15. S. O. Fetissov, L. C. Byrne, H. Hassani, P. Ernfors, T. Hökfelt, Characterization of neuropeptide Y Y2 and Y5 receptor expression in the mouse hypothalamus. *J. Comp. Neurol.* **470**, 256–265 (2004).
16. M. Benevento, T. Hökfelt, T. Harkany, Ontogenetic rules for the molecular diversification of hypothalamic neurons. *Nat. Rev. Neurosci.* **23**, 611–627 (2022).
17. R. A. Romanov, A. Alpár, M. Zhang, A. Zeisel, A. Calas, M. Landry, M. Fuszard, S. L. Shirran, R. Schnell, Á. Dobolyi, M. Oláh, L. Spence, J. Mulder, H. Martens, M. Palkovits, M. Uhlen, H. H. Sitte, C. H. Botting, L. Wagner, S. Linnarsson, T. Hökfelt, T. Harkany, A secretagogin locus of the mammalian hypothalamus controls stress hormone release. *EMBO J.* **34**, 36–54 (2015).
18. A. G. Roseberry, H. Liu, A. C. Jackson, X. Cai, J. M. Friedman, Neuropeptide Y-mediated inhibition of proopiomelanocortin neurons in the arcuate nucleus shows enhanced desensitization in ob/ob mice. *Neuron* **41**, 711–722 (2004).
19. S. Pinto, A. G. Roseberry, H. Liu, S. Diano, M. Shanabrough, X. Cai, J. M. Friedman, T. L. Horvath, Rapid rewiring of arcuate nucleus feeding circuits by leptin. *Science* **304**, 110–115 (2004).
20. S. M. Sternson, G. M. G. Shepherd, J. M. Friedman, Topographic mapping of VMH → arcuate nucleus microcircuits and their reorganization by fasting. *Nat. Neurosci.* **8**, 1356–1363 (2005).
21. X. B. Gao, A. N. Van Den Pol, Melanin-concentrating hormone depresses L-, N-, and P/Q-type voltage-dependent calcium channels in rat lateral hypothalamic neurons. *J. Physiol.* **542**, 273–286 (2002).
22. Y. Li, X. B. Gao, T. Sakurai, A. N. Van den Pol, Hypocretin/orexin excites hypocretin neurons via a local glutamate neuron - A potential mechanism for orchestrating the hypothalamic arousal system. *Neuron* **36**, 1169–1181 (2002).
23. L. Y. Fu, C. Acuna-Goycolea, A. N. Van Den Pol, Neuropeptide Y inhibits hypocretin/orexin neurons by multiple presynaptic and postsynaptic mechanisms: Tonic depression of the hypothalamic arousal system. *J. Neurosci.* **24**, 8741–8751 (2004).
24. Q. Gao, G. Mezei, Y. Nie, Y. Rao, C. S. Choi, I. Bechmann, C. Leranth, D. Toran-Allerand, C. A. Priest, J. L. Roberts, X. B. Gao, C. Mobbs, G. I. Shulman, S. Diano, T. L. Horvath, Anorectic estrogen mimics leptin's effect on the rewiring of melanocortin cells and Stat3 signaling in obese animals. *Nat. Med.* **13**, 89–94 (2007).
25. J. K. Elmquist, R. S. Ahima, E. Maratos-Flier, J. S. Flier, C. B. Saper, Leptin activates neurons in ventrobasal hypothalamus and brainstem. *Endocrinology* **138**, 839–842 (1997).
26. C. F. Elias, C. E. Lee, J. F. Kelly, R. S. Ahima, M. Kuhar, C. B. Saper, J. K. Elmquist, Characterization of CART neurons in the rat and human hypothalamus. *J. Comp. Neurol.* **432**, 1–19 (2001).
27. C. F. Elias, C. Aschkenasi, C. Lee, J. Kelly, R. S. Ahima, C. Bjorbæk, J. S. Flier, C. B. Saper, J. K. Elmquist, Leptin differentially regulates NPY and POMC neurons projecting to the lateral hypothalamic area. *Neuron* **23**, 775–786 (1999).
28. N. Balthasar, R. Coppari, J. McMinn, S. M. Liu, C. E. Lee, V. Tang, C. D. Kenny, R. A. McGovern, S. C. Chua, J. K. Elmquist, B. B. Lowell, Leptin receptor signaling in POMC neurons is required for normal body weight homeostasis. *Neuron* **42**, 983–991 (2004).
29. G. Paxinos, The hypothalamus: Neural systems involved in feeding, irritability, aggression, and copulation in male rats. *J. Comp. Physiol. Psychol.* **87**, 110–119 (1974).
30. G. A. Tannenbaum, G. Paxinos, D. Bindra, Metabolic and endocrine aspects of the ventromedial hypothalamic syndrome in the rat. *J. Comp. Physiol. Psychol.* **86**, 404–413 (1974).
31. M. A. Hofman, E. Fliers, E. Goudsmit, D. F. Swaab, Morphometric analysis of the suprachiasmatic and paraventricular nuclei in the human brain: Sex differences and age-dependent changes. *J. Anat.* **160**, 127–143 (1988).
32. E. A. Nillni, C. Vaslet, M. Harris, A. Hollenberg, C. Bjorbaek, J. S. Flier, Leptin regulates prothyrotropin-releasing hormone biosynthesis: Evidence for direct and indirect pathways. *J. Biol. Chem.* **275**, 36124–36133 (2000).
33. M. A. Cowley, R. G. Smith, S. Diano, M. Tschöp, N. Pronchuk, K. L. Grove, C. J. Strasburger, M. Bidlingmaier, M. Esterman, M. L. Heiman, L. M. Garcia-Segura, E. A. Nillni, P. Mendez, M. J. Low, P. Sotonyi, J. M. Friedman, H. Liu, S. Pinto, W. F. Colmers, R. D. Cone, T. L. Horvath, The distribution and mechanism of action of ghrelin in the CNS demonstrates a novel hypothalamic circuit regulating energy homeostasis. *Neuron* **37**, 649–661 (2003).
34. G. Q. Chang, V. Gaysinskaya, O. Karatayev, S. F. Leibowitz, Maternal high-fat diet and fetal programming: Increased proliferation of hypothalamic peptide-producing neurons that increase risk for overeating and obesity. *J. Neurosci.* **28**, 12107–12119 (2008).
35. K. Franke, T. Harder, L. Aerts, K. Melchior, S. Fahrenkrog, E. Rodekamp, T. Ziska, F. A. Van Assche, J. W. Dudenhausen, A. Plagemann, "Programming" of orexigenic and anorexigenic hypothalamic neurons in offspring of treated and untreated diabetic mother rats. *Brain Res.* **1031**, 276–283 (2005).
36. M. Nishi, Effects of early-life stress on the brain and behaviors: Implications of early maternal separation in rodents. *Int. J. Mol. Sci.* **21**, 7212 (2020).
37. A. Caqueret, C. Yang, S. Duplan, F. Boucher, J. L. Michaud, Looking for trouble: A search for developmental defects of the hypothalamus. *Horm. Res.* **64**, 222–230 (2005).
38. S. L. Fyffe, J. L. Neul, R. C. Samaco, H. T. Chao, S. Ben-Shachar, P. Moretti, B. E. McGill, E. H. Goulding, E. Sullivan, L. H. Tecott, H. Y. Zoghbi, Deletion of Mecp2 in Sim1-expressing neurons reveals a critical role for MeCP2 in feeding behavior, aggression, and the response to stress. *Neuron* **59**, 947–958 (2008).
39. B. E. McGill, S. F. Bundle, M. B. Yaylaoglu, J. P. Carson, C. Thaller, H. Y. Zoghbi, Enhanced anxiety and stress-induced corticosterone release are associated with increased Crh expression in a mouse model of Rett syndrome. *Proc. Natl. Acad. Sci. U.S.A.* **103**, 18267–18272 (2006).
40. A. F. M. van Abeelen, S. G. Elias, T. J. Roseboom, P. M. M. Bossuyt, Y. T. van der Schouw, D. E. Grobbee, C. S. P. M. Uiterwaal, Postnatal acute famine and risk of overweight: The dutch hungerwinter study. *Int. J. Pediatr.* **2012**, 1–9 (2012).

41. J. S. Huang, T. A. Lee, M. C. Lu, Prenatal programming of childhood overweight and obesity. *Matern. Child Health J.* **11**, 461–473 (2007).
42. S. D. Parlee, O. A. MacDougald, Maternal nutrition and risk of obesity in offspring: The Trojan horse of developmental plasticity. *Biochim. Biophys. Acta* **1842**, 495–506 (2014).
43. M. C. De Rosa, H. J. Glover, G. Stratigopoulos, C. A. LeDuc, Q. Su, Y. Shen, M. W. Sleeman, W. K. Chung, R. L. Leibel, J. Y. Altarejos, C. A. Doege, Gene expression atlas of energy balance brain regions. *JCI Insight.* **6**, e149137 (2021).
44. F. Inoue, W. L. Eckalbar, Y. Wang, K. K. Murphy, N. Matharu, C. Vaisse, N. Ahituv, Genomic and epigenomic mapping of leptin-responsive neuronal populations involved in body weight regulation. *Nat. Metab.* **1**, 475–484 (2019).
45. A. M. Bao, D. F. Swaab, The human hypothalamus in mood disorders: The HPA axis in the center. *IBRO Rep.* **6**, 45–98 (2019).
46. T. Shimogori, D. A. Lee, A. Miranda-Angulo, Y. Yang, H. Wang, L. Jiang, A. C. Yoshida, A. Kataoka, H. Mashiko, M. Avetisyan, L. Qi, J. Qian, S. Blackshaw, A genomic atlas of mouse hypothalamic development. *Nat. Neurosci.* **13**, 767–775 (2010).
47. Y. H. Zhang, M. Xu, X. Shi, X. L. Sun, W. Mu, H. Wu, J. Wang, S. Li, P. Su, L. Gong, M. He, M. Yao, Q. F. Wu, Cascade diversification directs generation of neuronal diversity in the hypothalamus. *Cell Stem Cell* **28**, 1483–1499.e8 (2021).
48. K. Tessmar-Raible, F. Raible, F. Christodoulou, K. Guy, M. Rembold, H. Hausen, D. Arendt, Conserved sensory-neurosecretory cell types in annelid and fish forebrain: Insights into hypothalamus evolution. *Cell* **129**, 1389–1400 (2007).
49. D. F. Swaab, Development of the human hypothalamus. *Neurochem. Res.* **20**, 509–519 (1995).
50. Y. Koutcherov, J. K. Mai, K. W. S. Ashwell, G. Paxinos, Organization of human hypothalamus in fetal development. *J. Comp. Neurol.* **446**, 301–324 (2002).
51. F. Schubert, J. M. George, M. Bhaskar Rao, Vasopressin and oxytocin content of human fetal brain at different stages of gestation. *Brain Res.* **213**, 111–117 (1981).
52. X. Zhou, Y. Lu, F. Zhao, J. Dong, W. Ma, S. Zhong, M. Wang, B. Wang, Y. Zhao, Y. Shi, Q. Ma, T. Lu, J. Zhang, X. Wang, Q. Wu, Deciphering the spatial-temporal transcriptional landscape of human hypothalamus development. *Cell Stem Cell* **29**, 328–343.e5 (2022).
53. X. Zhou, S. Zhong, H. Peng, J. Liu, W. Ding, L. Sun, Q. Ma, Z. Liu, R. Chen, Q. Wu, X. Wang, Cellular and molecular properties of neural progenitors in the developing mammalian hypothalamus. *Nat. Commun.* **11**, 4063 (2020).
54. T. J. Nowakowski, A. Bhaduri, A. A. Pollen, B. Alvarado, M. A. Mostajo-Radji, E. Di Lullo, M. Haeussler, C. Sandoval-Espinosa, S. J. Liu, D. Velmeshev, J. R. Ounadjela, J. Shuga, X. Wang, D. A. Lim, J. A. West, A. A. Leyrat, W. J. Kent, A. R. Kriegstein, Spatiotemporal gene expression trajectories reveal developmental hierarchies of the human cortex. *Science* **358**, 1318–1323 (2017).
55. A. A. Pollen, A. Bhaduri, M. G. Andrews, T. J. Nowakowski, O. S. Meyerson, M. A. Mostajo-Radji, E. Di Lullo, B. Alvarado, M. Bedolli, M. L. Dougherty, I. T. Fiddes, Z. N. Kronenberg, J. Shuga, A. A. Leyrat, J. A. West, M. Bershteyn, C. B. Lowe, B. J. Pavlovic, S. R. Salama, D. Haussler, E. E. Eichler, A. R. Kriegstein, Establishing cerebral organoids as models of human-specific brain evolution. *Cell* **176**, 743–756.e17 (2019).
56. A. Bhaduri, M. G. Andrews, W. Mancia Leon, D. Jung, D. Shin, D. Allen, D. Jung, G. Schmunk, M. Haeussler, J. Salma, A. A. Pollen, T. J. Nowakowski, A. R. Kriegstein, Cell stress in cortical organoids impairs molecular subtype specification. *Nature* **578**, 142–148 (2020).
57. U. C. Eze, A. Bhaduri, M. Haeussler, T. J. Nowakowski, A. R. Kriegstein, Single-cell atlas of early human brain development highlights heterogeneity of human neuroepithelial cells and early radial glia. *Nat. Neurosci.* **24**, 584–594 (2021).
58. A. Zeisel, H. Hochgerner, P. Lönnerberg, A. Johnsson, F. Memic, J. van der Zwan, M. Häring, E. Braun, L. E. Borm, G. La Manno, S. Codeluppi, A. Furlan, K. Lee, N. Skene, K. D. Harris, J. Hjerling-Leffler, E. Arenas, P. Ernfors, U. Marklund, S. Linnarsson, Molecular architecture of the mouse nervous system. *Cell* **174**, 999–1014.e22 (2018).
59. L. Steuernagel, B. Y. H. Lam, P. Klemm, G. K. C. Dowsett, C. A. Bauder, J. A. Tadross, T. S. Hitschfeld, A. del Rio Martin, W. Chen, A. J. de Solis, H. Fenselau, P. Davidsen, I. Cimino, S. N. Kohnke, D. Rimmington, A. P. Coll, A. Beyer, G. S. H. Yeo, J. C. Brüning, HypoMap-a unified single-cell gene expression atlas of the murine hypothalamus. *Nat. Metab.* **4**, 1402–1419 (2022).
60. E. S. Lein, M. J. Hawrylycz, N. Ao, M. Ayres, A. Bensinger, A. Bernard, A. F. Boe, M. S. Boguski, K. S. Brockway, E. J. Byrnes, L. Chen, L. Chen, T.-M. Chen, M. C. Chin, J. Chong, B. E. Crook, A. Czaplinska, C. N. Dang, S. Datta, N. R. Dee, A. L. Desaki, T. Desta, E. Diep, T. A. Dolbeare, M. J. Donelan, H.-W. Dong, J. G. Dougherty, B. J. Duncan, A. J. Ebbert, G. Eichele, L. K. Estin, C. Faber, B. A. Facer, R. Fields, S. R. Fischer, T. P. Fliss, C. Frensley, S. N. Gates, K. J. Glattfelder, K. R. Halverson, M. R. Hart, J. G. Hohmann, M. P. Howell, D. P. Jeung, R. A. Johnson, P. T. Karr, R. Kawal, J. M. Kidney, R. H. Knapik, C. L. Kuan, J. H. Lake, A. R. Laramee, K. D. Larsen, C. Lau, T. A. Lemon, A. J. Liang, Y. Liu, L. T. Luong, J. Michaels, J. J. Morgan, R. J. Morgan, M. T. Mortrud, N. F. Mosqueda, L. L. Ng, R. Ng, G. J. Orta, C. C. Overly, T. H. Pak, S. E. Parry, S. D. Pathak, O. C. Pearson, R. B. Puchalski, Z. L. Riley, H. R. Rockett, S. A. Rowland, J. J. Royall, M. J. Ruiz, N. R. Sarno, K. Schaffnit, N. V. Shapovalova, T. Sivisay, C. R. Slaughterbeck, S. C. Smith, K. A. Smith, B. I. Smith, A. J. Sodt, N. N. Stewart, K.-R. Stumpf, S. M. Sunkin, M. Sutram, A. Tam, C. D. Teemer, C. Thaller, C. L. Thompson, L. R. Varnam, A. Visel, R. M. Whitlock, P. E. Wohnoutka, C. K. Wolkey, V. Y. Wong, M. Wood, M. B. Yaylaoglu, R. C. Young, B. L. Youngstrom, X. F. Yuan, B. Zhang, T. A. Zwingman, A. R. Jones, Genome-wide atlas of gene expression in the adult mouse brain. *Nature* **445**, 168–176 (2007).
61. D. R. Ziegler, W. E. Cullinan, J. P. Herman, Distribution of vesicular glutamate transporter mRNA in rat hypothalamus. *J. Comp. Neurol.* **448**, 217–229 (2002).
62. G. Bowers, W. E. Cullinan, J. P. Herman, Region-specific regulation of glutamic acid decarboxylase (GAD) mRNA expression in central stress circuits. *J. Neurosci.* **18**, 5938–5947 (1998).
63. J. D. Hahn, O. Sporns, A. G. Watts, L. W. Swanson, Macroscale intrinsic network architecture of the hypothalamus. *Proc. Natl. Acad. Sci. U.S.A.* **116**, 8018–8027 (2019).
64. E. Sanz, A. Quintana, J. D. Deem, R. A. Steiner, R. D. Palmiter, G. S. McKnight, Fertility-regulating kiss1 neurons arise from hypothalamic pomc-expressing progenitors. *J. Neurosci.* **35**, 5549–5556 (2015).
65. A. H. Affinati, P. V. Sabatini, C. True, A. J. Tomlinson, M. Kirigiti, S. R. Lindsley, C. Li, D. P. Olson, P. Kievit, M. G. Myers, A. C. Rupp, Cross-species analysis defines the conservation of anatomically segregated VMH neuron populations. *eLife* **10**, e69065 (2021).
66. M. Liu, D. W. Kim, H. Zeng, D. J. Anderson, Make war not love: The neural substrate underlying a state-dependent switch in female social behavior. *Neuron* **110**, 841–856. e6 (2022).
67. E. L. Morris, A. P. Patton, J. E. Chesham, A. Crisp, A. Adamson, M. H. Hastings, Single-cell transcriptomics of suprachiasmatic nuclei reveal a Prokineticin-driven circadian network. *EMBO J.* **40**, e108614 (2021).
68. L. E. Mickelsen, W. F. Flynn, K. Springer, L. Wilson, E. J. Beltrami, M. Bolisetty, P. Robson, A. C. Jackson, Cellular taxonomy and spatial organization of the murine ventral posterior hypothalamus. *eLife* **9**, e58901 (2020).
69. M. A. Rossi, M. L. Basiri, Y. Liu, Y. Hashikawa, K. Hashikawa, L. E. Fenno, Y. S. Kim, C. Ramakrishnan, K. Deisseroth, G. D. Stuber, Transcriptional and functional divergence in lateral hypothalamic glutamate neurons projecting to the lateral habenula and ventral tegmental area. *Neuron* **109**, 3823–3837.e6 (2021).
70. A. C. Rupp, A. J. Tomlinson, A. H. Affinati, C. True, S. R. Lindsley, M. A. Kirigiti, A. MacKenzie, C. Li, L. B. Knudsen, D. P. Olson, P. Kievit, M. G. Myers Jr., Leptin-mediated suppression of food intake by conserved Glp1r-expressing neurons prevents obesity. bioRxiv 472115. 11 December 2021.
71. S. D. Lee, C. Priest, M. Bjursell, J. Gao, D. V. Arneson, I. S. Ahn, G. Diamante, J. E. van Veen, M. G. Massa, A. C. Calkin, J. Kim, H. Andersén, P. Rajbhandari, M. Porritt, A. Carreras, A. Ahnmark, F. Seeliger, I. Maxvall, P. Eliasson, M. Althage, P. Åkerblad, D. Lindén, T. A. Cole, R. Lee, H. Boyd, M. Bohlooly-Y, S. M. Correa, X. Yang, P. Tontonoz, C. Hong, IDOL regulates systemic energy balance through control of neuronal VLDLR expression. *Nat. Metab.* **1**, 1089–1100 (2019).
72. H. Flach, T. Basten, C. Schreiner, P. Dietmann, S. Greco, L. Nies, N. Roßmanith, S. Walter, M. Kühl, S. J. Kühl, Retinol binding protein 1 affects Xenopus anterior neural development via all-trans retinoic acid signaling. *Dev. Dyn.* **250**, 1096–1112 (2021).
73. V. A. Huynh-Thu, A. Irrthum, L. Wehenkel, P. Geurts, Inferring regulatory networks from expression data using tree-based methods. *PLOS ONE* **5**, e12776 (2010).
74. X. Zhang, G. Xiao, C. Johnson, Y. Cai, Z. K. Horowitz, C. Mennicke, R. Coffey, M. Haider, D. Threadgill, R. Eliscu, M. C. Oldham, A. Greenbaum, H. T. Ghashghaei, Bulk and mosaic deletions of Egfr reveal regionally defined gliogenesis in the developing mouse forebrain. *iScience* **26**, 106242 (2023).
75. C. A. G. Marshall, B. G. Novitch, J. E. Goldman, Olig2 directs astrocyte and oligodendrocyte formation in postnatal subventricular zone cells. *J. Neurosci.* **25**, 7289–7298 (2005).
76. W. Huang, A. Bhaduri, D. Velmeshev, S. Wang, L. Wang, C. A. Rottkamp, A. Alvarez-Buylla, D. H. Rowitch, A. R. Kriegstein, Origins and proliferative states of human oligodendrocyte precursor cells. *Cell* **182**, 594–608.e11 (2020).
77. H. Huang, J. L. Rubenstein, M. Qiu, Cracking the codes of cortical glial progenitors: Evidence for the common lineage of astrocytes and oligodendrocytes. *Neurosci. Bull.* **37**, 437–439 (2021).
78. J. Langlieb, N. Sachdev, K. Balderrama, N. Nadaf, M. Raj, E. Murray, J. Webber, C. Vanderburg, V. Gazestani, D. Tward, C. Mezias, X. Li, D. Cable, T. Norton, P. P. Mitra, F. Chen, E. Macosko, The cell type composition of the adult mouse brain revealed by single cell and spatial genomics. *bioRxiv*, (2023).
79. H. Yu, M. Rubinstein, M. J. Low, Developmental single-cell transcriptomics of hypothalamic POMC neurons reveal the genetic trajectories of multiple neuropeptidergic phenotypes. *eLife* **11**, e72883 (2022).
80. T. Ma, S. Z. H. Wong, B. Lee, G.-L. Ming, H. Song, Decoding neuronal composition and ontogeny of individual hypothalamic nuclei. *Neuron* **109**, 1150–1167.e6 (2021).
81. B. P. Shah, L. Vong, D. P. Olson, S. Koda, M. J. Krashes, C. Ye, Z. Yang, P. M. Fuller, J. K. Elmquist, B. B. Lowell, MC4R-expressing glutamatergic neurons in the paraventricular

hypothalamus regulate feeding and are synaptically connected to the parabrachial nucleus. *Proc. Natl. Acad. Sci. U.S.A.* **111**, 13193–13198 (2014).
82. H. Haas, P. Panula, The role of histamine and the tuberomamillary nucleus in the nervous system. *Nat. Rev. Neurosci.* **4**, 121–130 (2003).
83. N. Biglari, I. Gaziano, J. Schumacher, J. Radermacher, L. Paeger, P. Klemm, W. Chen, S. Corneliussen, C. M. Wunderlich, M. Sue, S. Vollmar, T. Klöckener, T. Sotelo-Hitschfeld, A. Abbasloo, F. Edenhofer, F. Reimann, F. M. Gribble, H. Fenselau, P. Kloppenburg, F. T. Wunderlich, J. C. Brüning, Functionally distinct POMC-expressing neuron subpopulations in hypothalamus revealed by intersectional targeting. *Nat. Neurosci.* **24**, 913–929 (2021).
84. C. Li, J. Navarrete, J. Liang, C. Lu, S. C. Funderburk, R. B. Chang, S. D. Liberles, D. P. Olson, M. J. Krashes, Defined paraventricular hypothalamic populations exhibit differential responses to food contingent on caloric state. *Cell Metab.* **29**, 681–694.e5 (2019).
85. K. P. Tolson, T. Gemelli, D. Meyer, U. Yazdani, J. Kozlitina, A. R. Zinn, Inducible neuronal inactivation of Sim1 in adult mice causes hyperphagic obesity. *Endocrinology* **155**, 2436–2444 (2014).
86. T. Yamanaka, A. Tosaki, H. Miyazaki, M. Kurosawa, Y. Furukawa, M. Yamada, N. Nukina, Mutant huntingtin fragment selectively suppresses Brn-2 POU domain transcription factor to mediate hypothalamic cell dysfunction. *Hum. Mol. Genet.* **19**, 2099–2112 (2010).
87. G. Mengod, E. Goudsmit, A. Probst, J. M. Palacios, *Chapter 4 In situ hybridization histochemistry in the human hypothalamus* (1992).
88. G. Mastorakos, I. Ilias, Maternal and fetal hypothalamic-pituitary-adrenal axes during pregnancy and postpartum. *Ann. N. Y. Acad. Sci.* **997**, 136–149 (2003).
89. R. D. Hodge, T. E. Bakken, J. A. Miller, K. A. Smith, E. R. Barkan, L. T. Graybuck, J. L. Close, B. Long, N. Johansen, O. Penn, Z. Yao, J. Eggermont, T. Höllt, B. P. Levi, S. I. Shehata, B. Aevermann, A. Beller, D. Bertagnolli, K. Brouner, T. Casper, C. Cobbs, R. Dalley, N. Dee, S. L. Ding, R. G. Ellenbogen, O. Fong, E. Garren, J. Goldy, R. P. Gwinn, D. Hirschstein, C. D. Keene, M. Keshk, A. L. Ko, K. Lathia, A. Mahfouz, Z. Maltzer, M. McGraw, T. N. Nguyen, J. Nyhus, J. G. Ojemann, A. Oldre, S. Parry, S. Reynolds, C. Rimorin, N. V. Shapovalova, S. Somasundaram, A. Szafer, E. R. Thomsen, M. Tieu, G. Quon, R. H. Scheuermann, R. Yuste, S. M. Sunkin, B. Lelieveldt, D. Feng, L. Ng, A. Bernard, M. Hawrylycz, J. W. Phillips, B. Tasic, H. Zeng, A. R. Jones, C. Koch, E. S. Lein, Conserved cell types with divergent features in human versus mouse cortex. *Nature* **573**, 61–68 (2019).
90. T. E. Bakken, N. L. Jorstad, Q. Hu, B. B. Lake, W. Tian, B. E. Kalmbach, M. Crow, R. D. Hodge, F. M. Krienen, S. A. Sorensen, J. Eggermont, Z. Yao, B. D. Aevermann, A. I. Aldridge, A. Bartlett, D. Bertagnolli, T. Casper, R. G. Castanon, K. Crichton, T. L. Daigle, R. Dalley, N. Dee, N. Dembrow, D. Diep, S. L. Ding, W. Dong, R. Fang, S. Fischer, M. Goldman, J. Goldy, L. T. Graybuck, B. R. Herb, X. Hou, J. Kancherla, M. Kroll, K. Lathia, B. van Lew, Y. E. Li, C. S. Liu, H. Liu, J. D. Lucero, A. Mahurkar, D. McMillen, J. A. Miller, M. Moussa, J. R. Nery, P. R. Nicovich, S. Y. Niu, J. Orvis, J. K. Osteen, S. Owen, C. R. Palmer, T. Pham, N. Plongthongkum, O. Poirion, N. M. Reed, C. Rimorin, A. Rivkin, W. J. Romanow, A. E. Sedeño-Cortés, K. Siletti, S. Somasundaram, J. Sulc, M. Tieu, A. Torkelson, H. Tung, X. Wang, F. Xie, A. M. Yanny, R. Zhang, S. A. Ament, M. M. Behrens, H. C. Bravo, J. Chun, A. Dobin, J. Gillis, R. Hertzano, P. R. Hof, T. Höllt, G. D. Horwitz, C. D. Keene, P. V. Kharchenko, A. L. Ko, B. P. Lelieveldt, C. Luo, E. A. Mukamel, A. Pinto-Duarte, S. Preissl, A. Regev, B. Ren, R. H. Scheuermann, K. Smith, W. J. Spain, O. R. White, C. Koch, M. Hawrylycz, B. Tasic, E. Z. Macosko, S. A. McCarroll, J. T. Ting, H. Zeng, K. Zhang, G. Feng, J. R. Ecker, S. Linnarsson, E. S. Lein, Comparative cellular analysis of motor cortex in human, marmoset and mouse. *Nature* **598**, 111–119 (2021).
91. K. Siletti, R. Hodge, A. M. Albiach, L. Hu, K. W. Lee, P. Lönnerberg, T. Bakken, S.-L. Ding, M. Clark, T. Casper, N. Dee, J. Gloe, C. D. Keene, J. Nyhus, H. Tung, A. M. Yanny, E. Arenas, E. S. Lein, S. Linnarsson, Transcriptomic diversity of cell types across the adult human brain. *Science* **382**, 6667 (2023).
92. T. Daley, A. D. Smith, Predicting the molecular complexity of sequencing libraries. *Nat. Methods* **10**, 325–327 (2013).
93. T. Stuart, A. Butler, P. Hoffman, C. Hafemeister, E. Papalexi, W. M. Mauck, Y. Hao, M. Stoeckius, P. Smibert, R. Satija, Comprehensive integration of single-cell data. *Cell* **177**, 1888–1902.e21 (2019).
94. R. C. Bandler, I. Vitali, R. N. Delgado, M. C. Ho, E. Dvoretskova, J. S. Ibarra Molinas, P. W. Frazel, M. Mohammadkhani, R. Machold, S. Maedler, S. A. Liddelow, T. J. Nowakowski, G. Fishell, C. Mayer, Single-cell delineation of lineage and genetic identity in the mouse brain. *Nature* **601**, 404–409 (2022).
95. E. A. Newman, D. Wu, M. M. Taketo, J. Zhang, S. Blackshaw, Canonical Wnt signaling regulates patterning, differentiation and nucleogenesis in mouse hypothalamus and prethalamus. *Dev. Biol.* **442**, 236–248 (2018).
96. A. Bhaduri, C. Sandoval-Espinosa, M. Otero-Garcia, I. Oh, R. Yin, U. C. Eze, T. J. Nowakowski, A. R. Kriegstein, An atlas of cortical arealization identifies dynamic molecular signatures. *Nature* **598**, 200–204 (2021).
97. M. Peng, B. Wamsley, A. G. Elkins, D. H. Geschwind, Y. Wei, K. Roeder, Cell type hierarchy reconstruction via reconciliation of multi-resolution cluster tree. *Nucleic Acids Res.* **49**, e91 (2021).
98. E. Sjöstedt, W. Zhong, L. Fagerberg, M. Karlsson, N. Mitsios, C. Adori, P. Oksvold, F. Edfors, A. Limiszewska, F. Hikmet, J. Huang, Y. Du, L. Lin, Z. Dong, L. Yang, X. Liu, H. Jiang, X. Xu, J. Wang, H. Yang, L. Bolund, A. Mardinoglu, C. Zhang, K. von Feilitzen, C. Lindskog, F. Pontén, Y. Luo, T. Hökfelt, M. Uhlén, J. Mulder, An atlas of the protein-coding genes in the human, pig, and mouse brain. *Science* **367**, eaay5947 (2020).
99. R. B. Patterson-Cross, A. J. Levine, V. Menon, Selecting single cell clustering parameter values using subsampling-based robustness metrics. *BMC Bioinform.* **22**, 39 (2021).
100. J. Cao, M. Spielmann, X. Qiu, X. Huang, D. M. Ibrahim, A. J. Hill, F. Zhang, S. Mundlos, L. Christiansen, F. J. Steemers, C. Trapnell, J. Shendure, The single-cell transcriptional landscape of mammalian organogenesis. *Nature* **566**, 496–502 (2019).
101. T. D. Sherman, T. Gao, E. J. Fertig, CoGAPS 3: Bayesian non-negative matrix factorization for single-cell analysis with asynchronous updates and sparse data structures. *BMC Bioinformatics* **21**, 453 (2020).
102. M. Crow, A. Paul, S. Ballouz, Z. J. Huang, J. Gillis, Characterizing the replicability of cell types defined by single cell RNA-sequencing data using MetaNeighbor. *Nat. Commun.* **9** (2018).
103. G. Sharma, C. Colantuoni, L. A. Goff, E. J. Fertig, G. Stein-O'Brien, projectR: An R/Bioconductor package for transfer learning via PCA, NMF, correlation and clustering. *Bioinformatics* **36**, 3592–3593 (2020).
104. B. J. Molyneaux, L. A. Goff, A. C. Brettler, H. H. Chen, J. R. Brown, S. Hrvatin, J. L. Rinn, P. Arlotta, DeCoN: Genome-wide analysis of In Vivo transcriptional dynamics during pyramidal neuron fate selection in neocortex. *Neuron* **85**, 275–288 (2015).
105. M. J. Lewis, M. R. Barnes, K. Blighe, K. Goldmann, S. Rana, J. A. Hackney, N. Ramamoorthi, C. R. John, D. S. Watson, S. K. Kummerfeld, R. Hands, S. Riahi, V. Rocher-Ros, F. Rivellese, F. Humby, S. Kelly, M. Bombardieri, N. Ng, M. DiCicco, D. van der Heijde, R. Landewé, A. van der Helm-van Mil, A. Cauli, I. B. McInnes, C. D. Buckley, E. Choy, P. C. Taylor, M. J. Townsend, C. Pitzalis, Molecular portraits of early rheumatoid arthritis identify clinical and treatment response phenotypes. *Cell Rep.* **28**, 2455–2470.e5 (2019).
106. P. Langfelder, S. Horvath, WGCNA: An R package for weighted correlation network analysis. *BMC Bioinformatics* **9**, 559 (2008).

Acknowledgments: We thank O. White and the Neuroscience Multi-Omic Archive team and Ronna Hertzano and the gEAR/NeMO Analytics team, respectively, for their assistance in building and hosting the data resources and web browsers that accompany this study. Some primary human tissue was obtained from the HDBR, with special thanks to S. Lisgo and M. Crosier. We would also like to thank S. Linnarsson for assistance with obtaining and processing human adult samples. **Funding:** This work was supported by the National Institutes of Health grants U01MH114825 (to A.R.K.), U01MH114812 (to E.L.), R24MH114788 [O. White, principal investigators (PIs)], R24MH114815 (O. White and R. Hertzano, PIs), and R01DC019370 (R. Hertzano, PI). C.A.D. is supported by the Frontiers program of the Russell Berrie Foundation, New York Obesity Research Center, P30 DK026687-43 and DK52431-25. **Author contributions:** Conceptualization: B.R.H., H.J.G., T.L.B., C.A.D., and S.A.A. Methodology: B.R.H., S.A.A., and C.C. Investigation: B.R.H. and H.J.G. Resources: A.B., K.S., R.H., E.L., and A.R.K. Supervision: C.A.D. and S.A.A. Writing—original draft: B.R.H., H.JG., C.A.D., and S.A.A. Writing—review and editing: All authors. **Competing interests:** A.R.K. is a cofounder and board member of Neurona Therapeutics. The other authors declare that they have no competing interests. **Data and materials availability:** All data needed to evaluate the conclusions of the paper are present in the paper and/or the Supplementary Materials. The data analyzed in this study were produced through the Brain Initiative Cell Census Network (BICCN:RRID:SCR_015820) and deposited in the NEMO Archive (RRID:SCR_016152) under identifier nemo:dat-917e9vs accessible at https://assets.nemoarchive.org/dat-917e9vs. Data can be explored on NeMO Analytics (https://nemoanalytics.org/p?l=a856c14e&g=gad2). Code availability: Code is presented on Zenodo (10.5281/zenodo.10019390) and GitHub (https://github.com/brianherb/HumanHypoDev2Adult).

Submitted 2 November 2022
Accepted 24 October 2023
Published 8 November 2023
10.1126/sciadv.adf6251